

**FEASIBILITY EXPERIMENTS TOWARD A HIGH-THROUGHPUT  
MICROSCOPE PLATFORM FOR NEUROSCIENCE RESEARCH IN  
*C. ELEGANS***

A Thesis Presented

By

Yao Wang

to

The Department of Bioengineering

in partial fulfillment of the requirements

for the degree of

Master of Science

in the field of

Bioimaging & Signal Processing

Northeastern University

Boston, Massachusetts

April 2018

## ABSTRACT

Lesion conditioning in neurons activates cellular mechanisms that significantly enhance neuro-regeneration. A study recently established the roundworm *C. elegans* as a powerful model for the rapid discovery of genes underlying lesion conditioning, which is currently impractical in vertebrates. Even so, a complete search for regeneration genes requires surgery and reimaging of a fluorescent neuron in more than 30,000 animals, which is impractical. Thus, a high-throughput surgery and reimaging platform, or specifically, a new integrated microscope platform for rapid immobilization, imaging, and optical surgery of *C. elegans*, would enable this genetic search. Achievement of this goal requires the acceleration of two time-consuming steps: animal immobilization and precise neuronal microscopy. This will be accomplished through two specific goals: 1. Develop a microscope stage to readily immobilize many animals for *in vivo* imaging. 2. Enable robust automation of microscopy by improving neuron-background contrast. For Goal 1, *C. elegans* will be immobilized by thermoelectrically cooling them directly on their cultivation plates, instead of mounting them to slides. For Goal 2, a patterned illumination approach will enhance the signal-to-background contrast by illuminating mainly the axon and dendrites of the desired neuron, while minimizing the excitation power that illuminates extremely bright cell bodies. Minimizing this excitation will help reduce scattered haze that blurs the axons and dendrites. This approach will enable the rapid and straightforward microscopy of large populations necessary for a gene search. In this paper, we show some primary simulation and experiments to demonstrate that: 1. It is possible to immobilize *C. elegans* on their cultivation agar plate, based on thermal simulation on the cooling stage followed by real tests utilizing Peltier stages. 2. It is possible to achieve arbitrary patterned illumination by a fast tissue responsivity segmentation algorithm, followed by Spatial Light Modulator (SLM) being integrated into the microscope illumination pathway. These experiments and simulation results presented in this paper establish the feasibility of achieving goal 1 and goal 2, and thus it is promising to build a high-throughput microscope platform for neuroscience research in *C. elegans*.

## ACKNOWLEDGMENTS

I would express my greatest gratitude to my master advisor and lab PI, Dr. Samuel Chung, assistant professor at the bioengineering department. My knowledge of Neuroscience and Biophotonics was nearly blank when I entered Dr. Chung's lab. By tirelessly tutoring me for almost two years, I got the chance to get into those areas and thus have the chance and knowledge to finish this master thesis. I am very grateful to Dr. Chung, for leading me to this fantastic research area and offering me the chance to do frontier research.

I would also like to thank Dr. Qianqian Fang, his Biomedical Imaging class was very inspiring, and I learned a lot from this course, some of the contents of that class are quite helpful in doing my thesis. Thank Dr. Vivek Venkatachalam, for willing to devote his time to help in give me very valuable comments on my thesis.

I would like to thank Samuel Urena and Noa Grooms, we are good partners in Dr. Chung's lab and did a lot of experiments together. They are always willing to help on not only experiments but also many other academic studies. Erik Jaklitsch, he helped me in doing the cooling stage project and made the process much faster, I appreciate that a lot.

Also, I want to thank Zhibin Chen, an undergraduate student from the biology department. We joined Dr. Chung's lab together while I was very unfamiliar with all those biological experiments in the lab. She helped me a lot about how to do those experiment, and thus I got familiar with most lab techniques much faster.

I would also like to acknowledge Dr. Jerome Mertz and his Ph.D. student Sheng Xiao, at Boston University, for lending us their spatial light modulator to us, so we were able to try some light patterning experiment. Dr. Charles DiMarzio and his Ph.D. student Danny Zhao, at ECE department, NEU, for lending us their polarizers for the same light patterning experiment.

# TABLE OF CONTENTS

<b>ABSTRACT</b> .....	<b>ii</b>
<b>TABLE OF CONTENTS</b> .....	<b>iv</b>
<b>LIST OF FIGURES</b> .....	<b>vi</b>
<b>LIST OF TABLES</b> .....	<b>ix</b>
<b>1. INTRODUCTION</b> .....	<b>1</b>
<b>1.1 Overview</b> .....	<b>1</b>
<b>1.2 Ultimate Goal</b> .....	<b>3</b>
<b>1.3 Specific Technical Goals</b> .....	<b>3</b>
1.3.1    Goal 1: Reduced Preparation Time.....	4
1.3.2    Goal 2: Improved Image Contrast.....	7
<b>2. PLANNED SETUP</b> .....	<b>11</b>
<b>2.1 Cooling Stage</b> .....	<b>11</b>
<b>2.2 Active Illumination Microscopy</b> .....	<b>14</b>
<b>3. EXPERIMENTS</b> .....	<b>18</b>
<b>3.1 Cooling Stage Initial Experiments</b> .....	<b>18</b>
3.1.1    Cooling Stage Simulation .....	18
3.1.2    Peltier Testing .....	20
3.1.3    Cultivation Plate Cooling.....	23
<b>3.2 Active Illumination Microscopy (AIM) Initial Experiments</b> .....	<b>24</b>

3.2.1	Worm Identification.....	25
3.2.2	Slit Image.....	30
3.2.3	Microscope Patterned Illumination using SLM LC2002.....	32
3.2.4	Neuron Coarse Segmentation.....	35
<b>4.</b>	<b>SUMMARY.....</b>	<b>40</b>
<b>5.</b>	<b>REFERENCE.....</b>	<b>43</b>
<b>6.</b>	<b>APPENDIX.....</b>	<b>48</b>
<b>6.1</b>	<b>Macros in Nikon NIS-Elements.....</b>	<b>48</b>
<b>6.2</b>	<b>Nikon Software Development Kit (SDK).....</b>	<b>51</b>

## LIST OF FIGURES

<b>Figure 1 The 3D Model of ASJ in <i>C. elegans</i> (Cite from WormAtlas)</b> .....	2
<b>Figure 2 Laser Cutting on Axon and Dendrite (Neuron Image by Confocal Microscope)</b> .....	3
<b>Figure 3 Horizontally Arranged Worms on Covered Slide</b> .....	5
<b>Figure 4 Wide-field Image of GFP Labelled ASJ Neuron</b> .....	8
<b>Figure 5 Image Quality Comparison between Wide-field Image and Confocal Image</b> .....	9
<b>Figure 6 Schematic of A Commercially Available</b> .....	13
<b>Figure 7 The 3D Model of the Overall Cooling Stage Setup and Top View of the Cooling Stage without Liquid Cooler</b> .....	13
<b>Figure 8 Nikon Ti2 Inverted Microscope Beam Pathway with an SLM</b> .....	15
<b>Figure 9 3D Model of the Cooling Stage for Thermal Simulation</b> .....	18
<b>Figure 10 Thermal Simulation Result</b> .....	20
<b>Figure 11 Immersed Peltier Heatsink to Ice Bath/Water</b> .....	21
<b>Figure 12 With the hot surface of the Peltier pasted to large aluminum block, the cold surface reached -34.4°C, while the aluminum block reached only 23.7°C ..</b>	22

<b>Figure 13 Placement of Cultivation Plate on the Peltier .....</b>	<b>23</b>
<b>Figure 14 Temperature of Agar inside Cultivation Plate .....</b>	<b>24</b>
<b>Figure 15 WorMachine workflow. The software includes three main functions [24]26</b>	
<b>Figure 16 <i>C. elegans</i> and its Trails on Agar [50].....</b>	<b>27</b>
<b>Figure 17 Large Image of Worms on An Unseeded Agar Plate, the quantity was 1828</b>	
<b>Figure 18 Worm Identification using ImageProcessor in WorMachine, with a Track on Agar Incorrectly Identified as a Worm.....</b>	<b>28</b>
<b>Figure 19 The Features Extractor in WorMachine Successfully Identified the Nose and the Tail of a Worm in Our Experiment.....</b>	<b>29</b>
<b>Figure 20 Beam-path of using SLM to pattern light .....</b>	<b>30</b>
<b>Figure 21 Slit patterned illumination with 0.55 <math>\mu\text{m}</math> resolution. Thin slit at field stop illuminates dye through 1.4 NA, 60x objective. Plot shows intensity along the gray line.....</b>	<b>31</b>
<b>Figure 22 Beam Path Scheme for Real Illumination Patterning.....</b>	<b>33</b>
<b>Figure 23 Real Illumination Patterning Setup .....</b>	<b>34</b>
<b>Figure 24 SLM Input Image and Camera Output Image. There is a blurry ghost image in (b) due to SLM LC2002 damage.....</b>	<b>34</b>
<b>Figure 25 Images with 10%, 40% and 80% intensity in turn, on <i>C. elegans</i>' ASJ neuron. All images are in 16-bit depth, with the same contrast adjustment. ....</b>	<b>37</b>
<b>Figure 26 Ratio Heatmap Calculated from the Images Set .....</b>	<b>37</b>

<b>Figure 27 Segmented Image Using the Above Images Set.....</b>	<b>39</b>
<b>Figure 28 The Scheme of Our Live Feedback Algorithm.....</b>	<b>50</b>
<b>Figure 29 The Macro Pane in Our Nikon NIS-Elements .....</b>	<b>51</b>
<b>Figure 30 Microscope Controlling App Designed in Matlab App Designer .....</b>	<b>52</b>



## LIST OF TABLES

<b>Table 1 Thermal conductivity W/(m K) of Materials Used in Cooling Stage, at 25 °C</b> .....	19
<b>Table 2 Attributes of the Multi-Stage Peltier We Use</b> .....	20
<b>Table 3 Comparison between LC2012 and LC2002</b> .....	32

# 1. INTRODUCTION

## 1.1 Overview

Following a traumatic injury, the mammalian central nervous system (CNS) typically fails to regenerate, leading to incurable conditions with immense healthcare burdens. A striking exception is a remarkable effect called lesion conditioning, where injury to a neuron's peripheral fiber activates cellular mechanisms to greatly enhance neuroregeneration [1, 2]. In lesion conditioning, a lesion of a neuron's peripheral sensory axon activates cellular mechanisms to enhance neuroregeneration and neuroprotection [2]. Originally shown to accelerate regeneration [3] and recovery of function [4] in the peripheral nervous system (PNS), lesion conditioning also drives CNS regeneration [5] past the highly inhibitory lesion site [6]. Identifying critical components of lesion conditioning pathways would represent a crucial step toward improving health outcomes.

However, due to the complexity of the neuron system of the human or vertebrate animal, it is hard to identify proper gene pathways involved in lesion conditioning. That is why, even though vertebrate models have already been used to research lesion conditioning for over four decades, we still lack a systematic and comprehensive identification of its genetics. To address this gap in knowledge, Dr. Samuel Chung's laboratory recently established a novel model in the nematode *C. elegans* [7].

*C. elegans*, or *Caenorhabditis elegans*, is a free-living transparent nematode, about 1 mm in length [8]. At 20°C, the wild strain of *C. elegans* (N2) has an average lifespan around 2–3 weeks and a generation time of 3 to 4 days. *C. elegans* was the first

multicellular organism to have its whole genome sequenced, in 1998 [9]. Moreover, many *C. elegans* genes can function similarly to mammalian genes. In summary, *C. elegans* is transparent in bright field (BF) imaging, has a short lifespan for reproducing, is small for easily culturing in a large number, and has genetic relevance to humans.

Compared to researching in vertebrate model animals, gene screening towards lesion conditioning in *C. elegans* is a high-throughput approach which could define all genes involved in triggering lesion conditioning. In order to trigger lesion condition in *C. elegans*, we use femtosecond laser surgery to cut both the axon and the dendrite of the ASJ neuron of *C. elegans* [10]. In Dr. Chung's 2016 PNAS paper, he modeled lesion conditioning in the ASJ neuron in the nose of *C. elegans* [7].

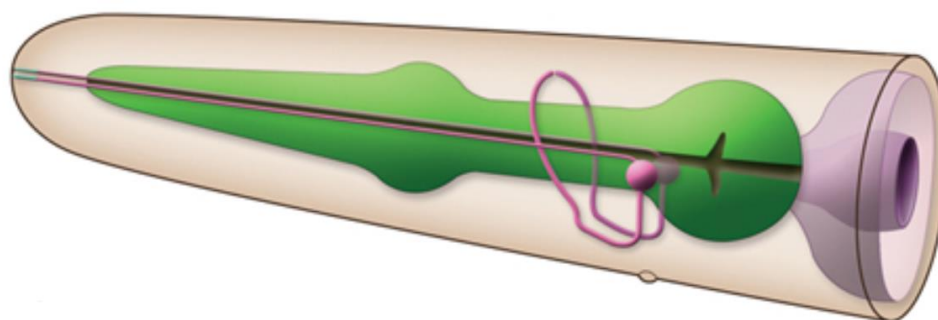


**Figure 1 The 3D Model of ASJ in *C. elegans*** (Cite from WormAtlas)

Femtosecond laser ablation can selectively dissect subcellular components of the *C. elegans* neuronal circuit with sub-micrometer precision [10, 11]. It can cut the axons and dendrites of the neuron without collateral damage. By using femtosecond laser surgery in *C. elegans*, researchers have greater control on creating neuronal lesions, which will lead to a faster verification of whether a gene is involved in lesion conditioning. In our lab, we will continuously use laser surgery to trigger lesion conditioning for gene screening in *C. elegans*.

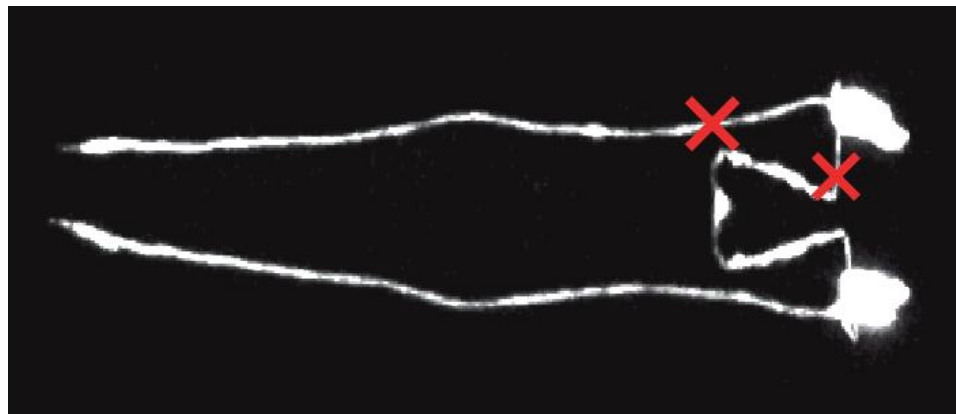


**Figure 2 Laser Cutting on Axon and Dendrite** (Neuron Image by Confocal Microscope)

## 1.2 Ultimate Goal

Using *C. elegans* for lesion conditioning gene screening will expedite the overall neuron regeneration research in vertebrate animals. However, considering the large number (usually > 30,000) of animals we need to screen for those genes [12], we seek for a faster way to do femtosecond laser surgery in *C. elegans*.

Currently, the overall laser surgery on each worm takes roughly 5 minutes of a researcher's time. For screening on 30,000 worms, it takes about 150,000 minutes, or 2,500 hours of a researcher's time. This is too slow and needs acceleration. We aim to accelerate the laser surgery by ten times, so that it takes roughly 0.5 minutes of a researcher's time on each worm. In order to achieve this, we want to make the whole laser surgery procedure more straightforward and more accessible. Thus, our ultimate goal is to computer automate the imaging and laser surgery procedures, with minimal human participation. This automated laser surgery and microscopy platform will accelerate neuroscience research.

## 1.3 Specific Technical Goals

To achieve our desired automated laser surgery and microscopy platform, we need to achieve two specific goals. Goal 1 is to reduce preparation time for imaging and surgery; Goal 2 is to improve image contrast by a novel wide-field Active Illumination Microscopy (AIM), which was invented by Jerome Mertz for scanning microscopy[13].

With the accomplishment of these two goals, and combining some other existing methods, we hope to achieve an automated laser surgery platform, which can be used for high-throughput neuroscience research worldwide.

### 1.3.1 Goal 1: Reduced Preparation Time

Compared to gene screening in vertebrate animal, screening in *C. elegans* is already much faster. Even so, a complete search for lesion conditioning genes requires laser surgery and reimaging of a fluorescent neuron in more than 30,000 animals [12]. Thus, reducing the overall screening time is greatly needed.

For laser surgery in worms, we need to first image them to find the target locations on its axon and dendrites; then, we move to location where the laser spot will shoot. After this, we turn on the laser beam and the laser will shoot the location we chose. In both our lab and many other labs who are doing imaging and worm handling of *C. elegans* by using wide-field microscopes, the imaging procedure is similar, as described below:

Stage 1: Align Laser (depending on the laser's condition)

Stage 2: Mount *C. elegans* to slide for imaging on an Inverted Microscope (like Nikon Ti2).

1. Make agar solution with anesthetic
2. Heat up the agar solution
3. Drop agar to the aluminum block and cover with slide to make a thin agar pad
4. Pick roughly 20 worms from culture plate and put them to the agar on slide(Do note

that: Worms are tiny)

5. Arrange all worms to one direction(Do note that: Worms are tiny) (**Figure 3**)
6. Cover the slide with coverslip and seal it

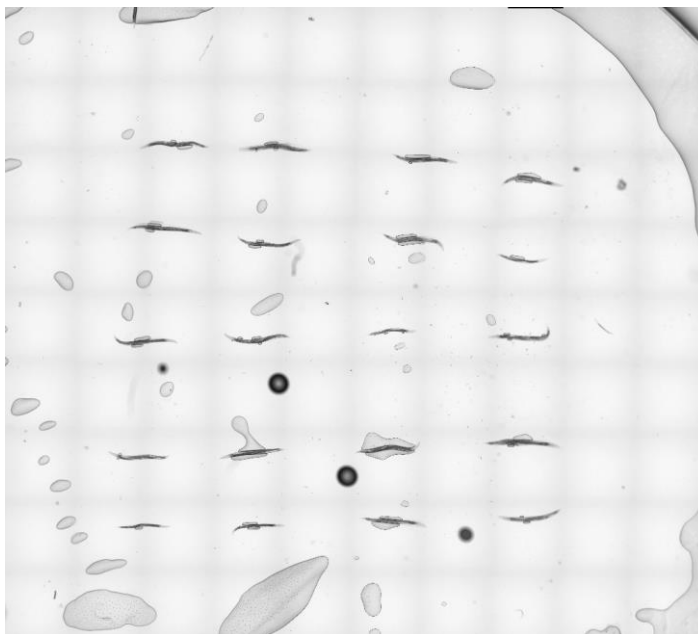


**Figure 3 Horizontally Arranged Worms on Covered Slide**

#### Stage 3: Image Worms and Laser Surgery

1. Place Slide on Microscope Stage
2. Find the nose of a worm, go to GFP
3. Focus to right Z plane
4. Move the laser spot to the location we want to shoot
5. Turn on laser beam to shoot

#### Stage 4: Move Worms Back to its Culturing Plate

1. Pick up worm after surgery from slide and immerse them in buffered solution
2. Wait roughly half an hour
3. Pick worms from buffered solution back to their culturing plate

For stage 1, aligning laser is a one-time job, once aligned, there is no need to align it

anymore within a period of time.

In general, a researcher consumes roughly 80% of his/her total time in stage 2 and stage 4. For example, if we need to shoot 20 worms, we spend nearly half an hour in completing stage 2. For stage 3, with the usage of Nikon NIS-Elements software (Nikon's microscope controlling software) installed in our lab computer, we can finish laser cutting of 20 worms in roughly 20 mins. For stage 4, even if we do not count the worm recovery waiting time, we still need to devote roughly 40 mins on processing, with the risk of losing a few worms during handling.

From above, we can calculate the experiment time on each worm is roughly 5 mins.

The purpose of our experiment is to cut a worm's neuron with the laser beam. Ideally, the only necessary procedure should be stage 3, which is 'Image Worms and Laser Surgery'. However, in order to image and cut neuron, worms must be immobilized. Also, for high magnification imaging, worms must be mounted on a slide, so it can be imaged by a high magnification objective on an inverted microscope. Mounting and immobilization of worms and its accompanying worm recovering post-surgery need enormous effort[14].

As Leica recently developed a stereomicroscope objective that allows subcellular-resolution, non-contact imaging; mounting worms become no longer necessary. But we still cannot skip the worm immobilization procedure. Other researchers who are working on *C. elegans* had figured out some alternative ways to immobilize worms. Recently-developed techniques immobilize animals by suction [15], clamping [16], and cooling [17, 18], in microfluidics (thin polymer channels) and multi-well plates. While these techniques have fluorescence sorting speeds up to 1000 worms/h [17], most *C. elegans* laboratories continue to perform microscopy by mounting animals on slides for several reasons. These techniques are challenging to learn, need significant fine-tuning of the microfluidics, and

require equipment that is not common in biological laboratories. Moreover, microfluidics—and some anesthetics—do not sufficiently immobilize regions near the oscillating nose and pumping pharynx, where our target neuron is located. Thus, we still have no suitable immobilization techniques for our experiment and must continue to use agar with anesthetic on a slide, to immobilize *C. elegans*, which is why we cannot skip stage 2 and stage 4.

Furthermore, using a slide for imaging has another problem. Slides often contain bubbles, which degrades imaging (**Figure 3**). This problem reduces the success rate of worm identification when using some existing algorithms.

In summary, these problems give us our Goal 1: reduced preparing time for worm surgery, or specifically, skip stage 2 and stage 4 if possible.

### 1.3.2 Goal 2: Improved Image Contrast

Like many other neuroscience labs, we are using a wide-field inverted Epi-fluorescence microscope (Nikon Ti2) for imaging. Unlike confocal microscope [19] or multi-photon microscope [20], a wide-field microscope cannot reject scattering light or out-of-focus light[21], which makes its image quality inferior to those scanning microscopes.

As can be seen in **Figure 4**, in a wide-field image, the cell body is extremely bright, usually 10x brighter than axon and dendrite, and generates haze that obscures its nearby axon and dendrites. This is a severe problem because laser surgeries are usually done in the region near the cell body.



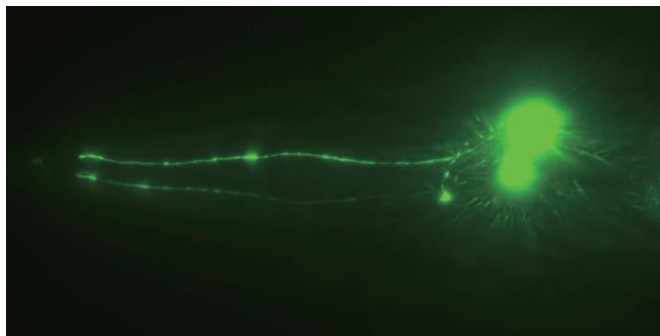


**Figure 4 Wide-field Image of GFP Labelled ASJ Neuron**

To automate laser surgery, the computer needs to first identify and locate worms on their cultivation agar. There are many existing methods to complete this task[22-25]. Then it comes to the core part; the computer should have the ability to segment the whole image to at least four categories: axon, dendrites, cell body, and background. After segmentation, the computer can trace the neuron [26] [27, 28] and then easily decide an optimal location to shoot at, by just calculating the length from a cell body.

There are numerous existing approaches for neuron segmentation published[29-32]. Those papers provide us several user-friendly software for neuron segmentation. All those methods require good image quality to achieve their desired segmentation performance and accuracy. This is why images from a multi-photon microscope or confocal microscope are mostly used. However, both confocal and multi-photon microscopes are expensive and hard to use, thus most neuroscience research labs do not have these kinds of microscope and will continue to use wide-field microscopes. We contacted most of those researchers who published those segmentation methods, and confirmed that, with the wide-field image we have, it is impossible to achieve a reasonable segmentation, or the false positive rate will be high.

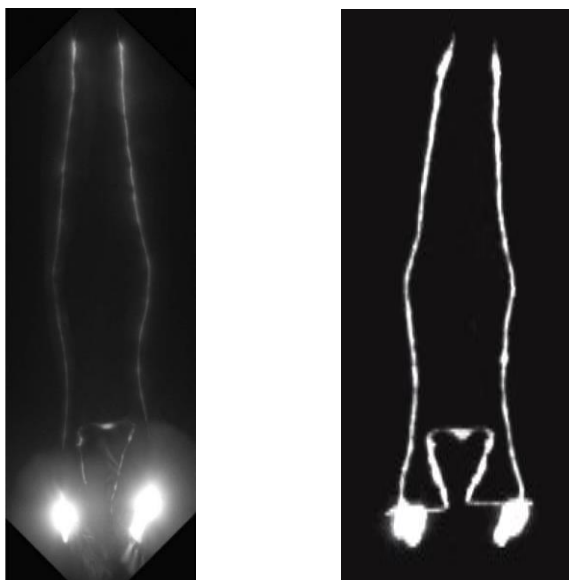


**Figure 5 Image Quality Comparison between Wide-field Image and Confocal Image**

With broadly used wide-field microscope setup, it is difficult to obtain a good quality image comparable to image from multi-photon or confocal. As so, it is difficult to get neuron segmentation done utilizing existing setups. However, if we could improve the wide-field image to the degree like multi-photon or confocal image, segmentation can easily be done by existing methods.

Improving the image quality, or signal-to-background ratio (SBR), of a wide-field image is a crucial step to success in completing automated laser surgery project. There are many methods to improve the wide-field image quality, like denoising [33, 34], deconvolution [35, 36], machine learning[37] and so on. Most of those methods can improve the image quality significantly, with computational post-processing. However, very few existing methods can improve the SBR directly on a wide-field microscope with live imaging.

We will implement a new variation of Active Illumination Microscopy (AIM) based on wide-field microscopy. Typical wide-field fluorescence microscope illuminates at a constant intensity on the whole field of view (FOV). AIM modulates illumination intensity

pixel by pixel, which forms a desired patterned illumination on the sample plane. Many people used active illumination on scanning microscope for faster imaging [38], achieving higher dynamic range [39], or minimizing photobleaching and maintaining a more constant emission intensity [40]. However, no one has utilized their technique to directly improve imaging contrast or determine the source of emission light (i.e., neuron or background). In consultation with professor Jerome Mertz 's group, we will utilize AIM to ascertain the source of emission light and improve the neuron/background contrast. This is our Goal 2: improving wide-field image contrast.

## 2. PLANNED SETUP

### 2.1 Cooling Stage

As discussed in this paper, we would like to skip the process of mounting worms to slides and subsequently moving them back to their cultivation plates after imaging; however, these steps cannot be currently avoided for the following reasons. Firstly, an inverted wide-field microscope needs a slide for imaging, because of its stage structure and the short working distance of their high numerical aperture (NA) objective. Secondly, for imaging and laser surgery, the worms need to be immobilized before they are placed onto the microscope, which is currently accomplished by applying an immobilizing anesthetic to the slide where the worms are positioned.

In order to skip stage 2 and stage 4, we aim to do the laser surgery directly on worms' daily culturing plate. It is not realistic to lay culturing plate directly on an inverted microscope stage for imaging. However, we can put plates under an upright microscope naturally, which has objectives with much longer working distance and reasonable NA. Then, by laser integration, we may do both the imaging and laser surgery on the upright microscope. Using the new developed Leica stereomicroscope objective, we can complete non-contact imaging and femtosecond laser surgery [41] of animals directly on their daily cultivation plates. However, we still need to immobilize worms on the plate for imaging and surgery.

We cannot put anesthetic directly to a culturing plate, because we do not want to destroy worms' culturing environment. Without anesthetic, we need to find some other

methods to immobilize worms on their culturing plate, without any long-term side effect on both plates and worms. Other people's research shows that exposing worms to cold temperatures, 2 °C -4 °C, can fully immobilize the worms [17]. Moreover, there is no long-term side effect if the exposing time is less than 4 hours[42]. Hence, it would be possible to use cold temperature to immobilize worms on their culturing plate, if we could chill down the whole plate to 2 °C -4 °C. As so, we will mount a cooling stage to a Leica upright stereomicroscope, to immobilize worms on their daily culturing plate, and then use the same microscope to image and laser shoot worms.

We will use a Peltier module as a cooling source for the whole cooling stage. The Peltier effect is named after French physicist Jean Charles Athanase Peltier, who discovered it in 1834. When current flows through a junction between two conductors/junctions of the Peltier, heat can be generated or removed at the junction. Thus, one end of the Peltier becomes hot and the other end becomes cold.

A typical Peltier heat pump involves multiple junctions in series, through which a current is driven (**Figure 6**). With enough current being inputted to the Peltier and the heat generated on the hot surface is efficiently removed, the Peltier's cold surface could become very cold. Then, if we can conduct heat from the cultivation plate to the cold surface of the Peltier, we can decrease the temperature of the whole plate significantly. If the agar inside plate become cold enough, worms on the agar surface will be completely immobilized.

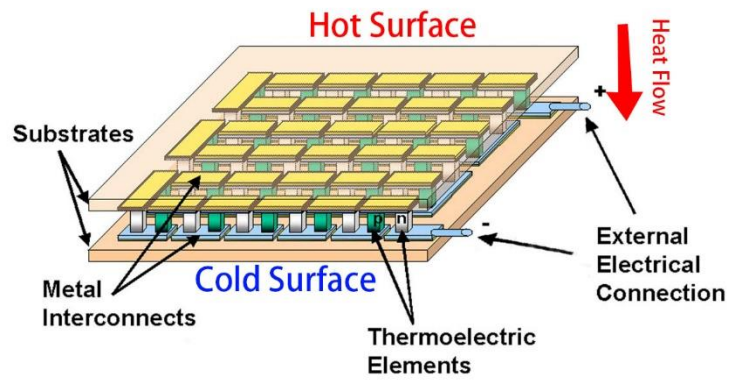


**Figure 6 Schematic of A Commercially Available Single Stage Peltier [43]**

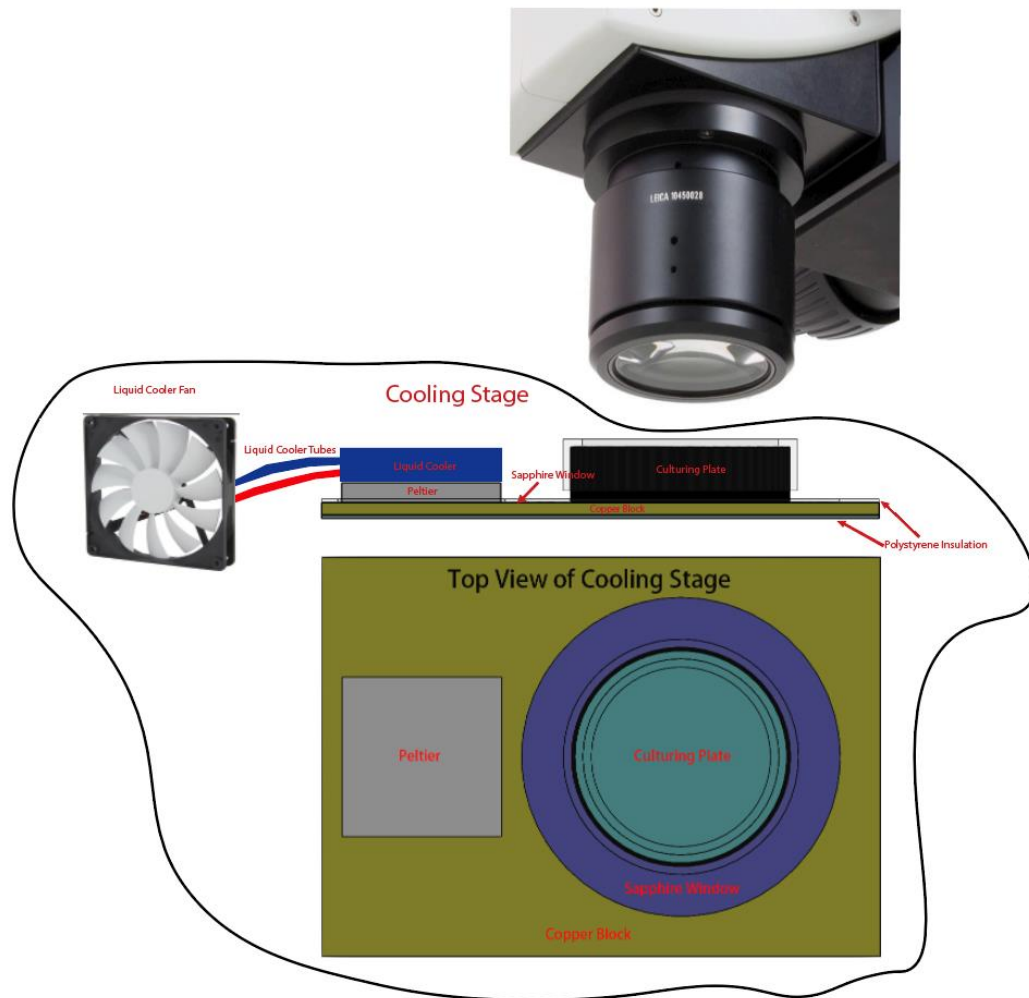


**Figure 7 The 3D Model of the Overall Cooling Stage Setup and Top View of the Cooling Stage without Liquid Cooler**

In **Figure 7**, we will first remove the heat generated on the hot surface of the Peltier with a liquid cooler. After this, we will apply the cold surface of the Peltier to a copper block. Then, there is a sapphire window placed in the opening of the copper block, so illumination light can pass through that window. The plate will be placed directly on the sapphire window. Thus, heat transfer from the Peltier pump will allow heat to be conducted first from the copper block, and then subsequently the sapphire window, plate, and agar inside, decreasing the temperature of the system efficiently enough to immobilize the worms. To keep the whole cooling stage more efficient, we also use some low thermal conductivity materials for thermal insulation.

In summary, the cooling stage comprises of seven major parts: cooling fan/heatsink or liquid cooler for cooling down the hot surface of the Peltier, adjustable power supply for the Peltier, thermometer for measuring agar surface temperature, the Peltier, copper block for conducting heat, sapphire window for conducting heat from cultivation plate to copper block, and some thermal insulation material to keep the cooling stage from being affected by room temperature.

## **2.2 Active Illumination Microscopy**

We will install a transmissive spatial light modulator (SLM) into the field stop of our Nikon Ti2 microscope. An SLM acts as a transmissive display screen and can transmit light in an arbitrary shape [44]. A field stop is a plane that is conjugate to the sample plane/objective focal plane. Therefore, whatever the shape of the illumination beam in the field stop plane is, there will be the same shape, magnified by a factor defined by condenser and objective, formed in the sample plane. For example, if the illumination shape in the

field stop plane is a ring, then the illumination onto the sample plane will be ring-like structured light.

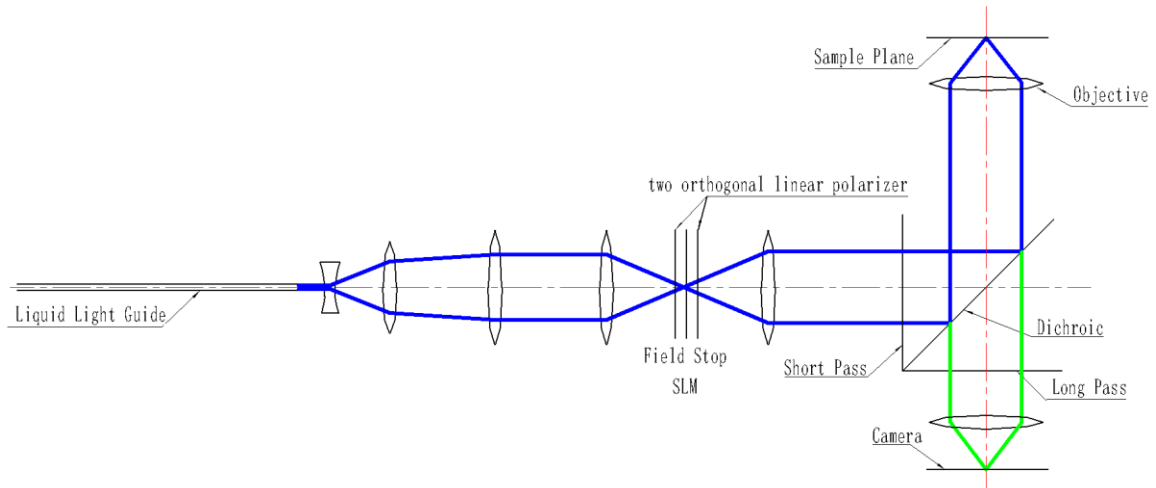


**Figure 8 Nikon Ti2 Inverted Microscope Beam Pathway with an SLM**

After installing an SLM in our inverted microscope Nikon Ti2 (**Figure 8**), we will use the SLM to pattern the illumination to a desired shape. We want the illumination shape to be patterned in such a way that, on the sample plane, it will shine at only those location that have an axon or dendrite, and the cell body and background areas should be receiving no excitation light (or shine minimal light to cell body for location reference). Thus, in ideal condition, only axons and dendrites of the neuron will be excited and radiate fluorescence, which will increase the SBR.

In order to allow the SLM to display the desired shape, we need a coarsely segmented image that we can input to the SLM. Existing segmentation methods for fluorescently-labeled tissues typically use emission intensity to distinguish neurons from its background. It might not be the best choice to use those methods for our wide-field fluorescence image segmentation, because the GFP expression in our sample is not uniform in the neuron. Also, regions surrounding bright neuronal tissue may scatter light into the camera and appear bright.



A better distinguishing parameter for segmentation can be calculated from the fluorescence ‘responsivity’. Analogously to photodetector responsivity, we define fluorescence responsivity as the emission intensity divided by the excitation intensity  $R = I^{\text{out}}/I^{\text{in}}$ .

When point scanning, the emission intensity will be dependent on the illumination intensity for neuronal tissue, but not for background. Thus, we expect that probing tissue “responsivity” pixel-by-pixel will allow us to ascertain if the pixel’s light originates directly from the neuron or from scattering.

Using the SLM, we will sequentially illuminate each location with several different intensities  $I^{\text{in}}$ . We will fit the correspond emission intensities  $I^{\text{out}}$  to a line and use the responsivity (i.e., the slope  $dI^{\text{out}}/dI^{\text{in}}$ ) as the parameter for segmentation, instead of the intensity normally utilized. We expect large slopes at locations containing fluorescent neuronal tissue but small slopes at background locations without fluorophores.

Thus, we will define a Responsivity Index (RI), which is an approximate measurement of the probability of a pixel being imaged on a neuron. A larger ratio between the low and high excitation levels should increase confidence in a pixel’s status. The RI is defined in Chapter 3.2.4.

We will measure pixel intensities and normalize to InSpeck Intensity Calibration fluorescent beads (Molecular Probes). While the camera chip manufacturer claims a 99.8% linearity in signal counts, we expect that there are very limited factors that will have unexpected influence on the slopes and RI.

Thresholding the RI will roughly segment the whole image to pixels with GFP and without GFP. Given that the cell body is much brighter than other pixels, we can merely use intensity thresholding to distinguish cell bodies.

By combining RI and intensity thresholding, we anticipate an output image that contains only axons and dendrites, with cell body and background not visible.

By inputting this new segmented image to the SLM in the microscope beam path, the SLM will pattern the excitation beam from wide-plane shape to axon with dendrites shape, and then this patterned light will only shine to the sample's axon and dendrites.

With the combination of SLM and segmentation algorithm, which will be a new wide-field active illumination microscopy, we will be able to acquire images with higher SBR in real time, which has never been done before.

## 3. EXPERIMENTS

### 3.1 Cooling Stage Initial Experiments

To test the feasibility of our cooling stage, we first modeled it in SolidWorks (Student Edition 2018) and used its thermal simulation to confirm whether our hypothetical setup could reach the desired temperature of below 4°C. After the simulation, we completed some experiments to confirm whether the actual setup conforms with the thermal simulation.

#### 3.1.1 Cooling Stage Simulation

Based on the dimension of our Leica M205 FA stereomicroscope and the working distance of its 1X and 5X objectives, we modeled the whole setup in Solidworks (**Figure 9**), except for the cooling fan/heatsink/liquid cooling components, which will be further decided during the experimental trials.

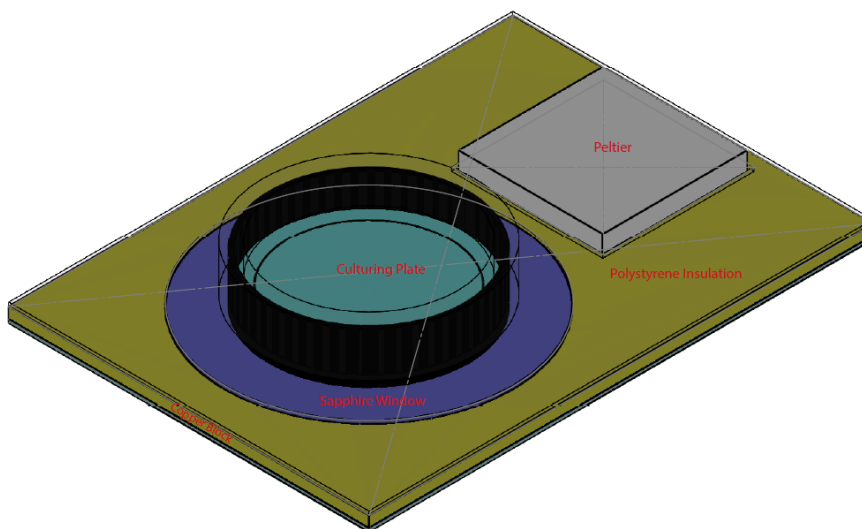


**Figure 9 3D Model of the Cooling Stage for Thermal Simulation**

For efficient thermal conduction from the Peltier cold surface to the agar inside cultivation plate, we want every material to have as high thermal conductivity as possible. Thus, we used copper as the main body of our cooling stage. Then, we excised a portion of the copper where the cultivation plate will be placed and replaced that portion with sapphire window for optical transparency, thus allowing for unhindered transmission of illumination light while possessing decent thermal conductivity. For thermal insulation from ambient room temperature, we used 2mm Polystyrene sheet, which possesses a low thermal conductivity and is readily available.

**Table 1 Thermal conductivity W/(m K) of Materials Used in Cooling Stage, at 25 °C**

<b>Material</b>	<b>Conductivity</b>
<b>Air</b>	0.0262
<b>Copper</b>	390
<b>Sapphire</b>	23
<b>Water</b>	0.6
<b>Polystyrene</b>	0.2256
<b>Agar</b>	0.58 <sup>[45]</sup>

We used SolidWorks Simulation module for the thermal simulation. We set the ambient temperature to 25 °C, higher than our real lab ambient temperature, to increase confidence in the translation of simulation results.

The thermal simulation (**Figure 10**) indicated that the optimal temperature of the cold surface of the Peltier should be maintained at -18 °C. The surface agar of our culturing plate is 2.6 °C on average, with a maximum temperature of 4.7 °C and minimum of 1.3 °C. This temperature range coincides with the Robinson's 2016 paper's research result [42]

and is promising for immobilizing worms on this cooling stage setup.

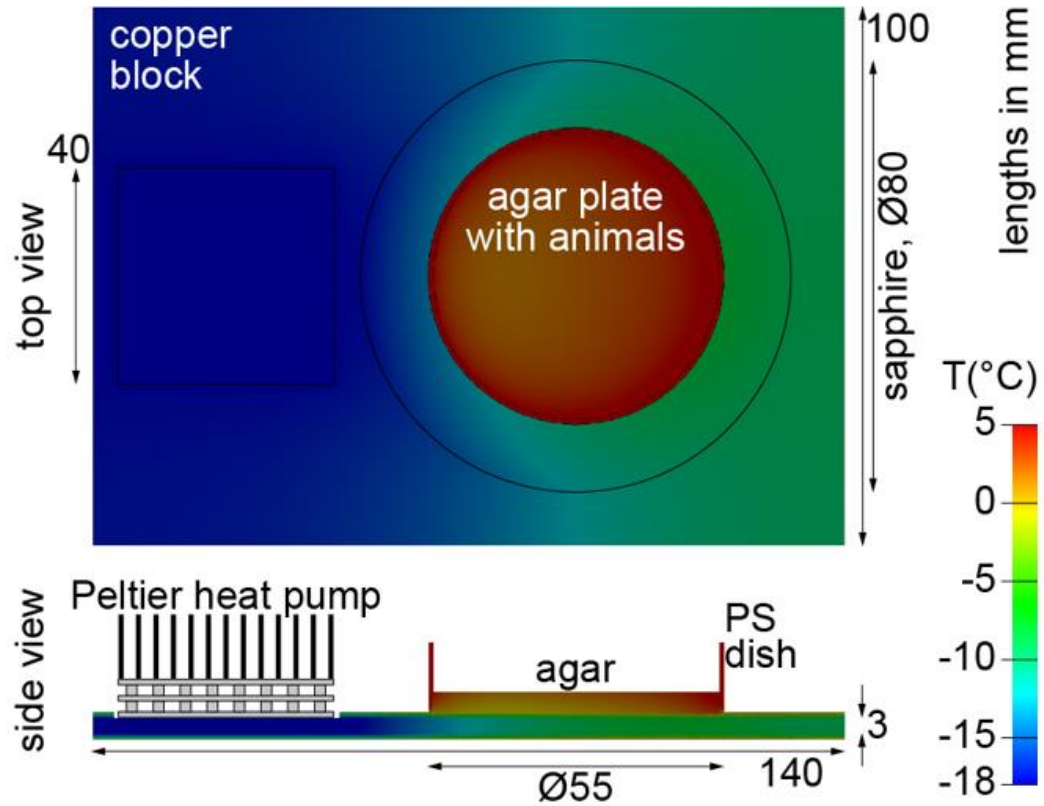


**Figure 10 Thermal Simulation Result**

### 3.1.2 Peltier Testing

The Peltier is the core component in our cooling stage setup, and its performance is extremely important. A Multi-Stage Peltier is composed of stacked single-stage Peltier, or cascaded to achieve higher temperature differences than that can be had with a single-stage Peltier [46]. Thus, we chose a multi-stage Peltier (CUI CP854705-2) for experiments.

**Table 2 Attributes of the Multi-Stage Peltier We Use**

Outline L x W x H	40.00mm x 40.00mm x 7.05mm
$Q_{\max}$ @ $T_h$	51.6W @ 27°C
$\Delta T_{\max}$ @ $T_h$	85°C @ 27°C
Current – Max	8.5A
Voltage - Max	16.1V
Resistance	1.65 Ohms
Operating Temperature	80°C

(Note:  $Q_{\max}$  is the maximum heat load the Peltier can transfer from the cold side to the hot side assuming it is running 100% efficient.  $\Delta T_{\max}$  is the most efficient temperature difference between the hot side and cold side, under no load.)

As we did not have an efficient enough cooling system (liquid cooler) to remove all of the heat generated by the hot surface of the Peltier, we had to use some ad hoc methods to test the performance of the Peltier.

The area of the hot surface of the Peltier itself is not adequate to dissipate all of the generated heat. Consequently, a heatsink must be used. The heatsink will aid in eliminating heat generated by the Peltier, and its efficiency in removing the heat determines the cooling performance of the Peltier [47].

Because the  $\Delta T_{\max}$  of our Peltier is  $85^{\circ}\text{C}$  under ideal conditions, we must make the hot surface of the Peltier as cool as possible to make the cold surface of the Peltier  $-18^{\circ}\text{C}$ , same as calculated in the thermal simulation. Therefore, we immersed the whole heatsink sitting on the hot surface of the Peltier to an ice bath, which is  $0^{\circ}\text{C}$ .

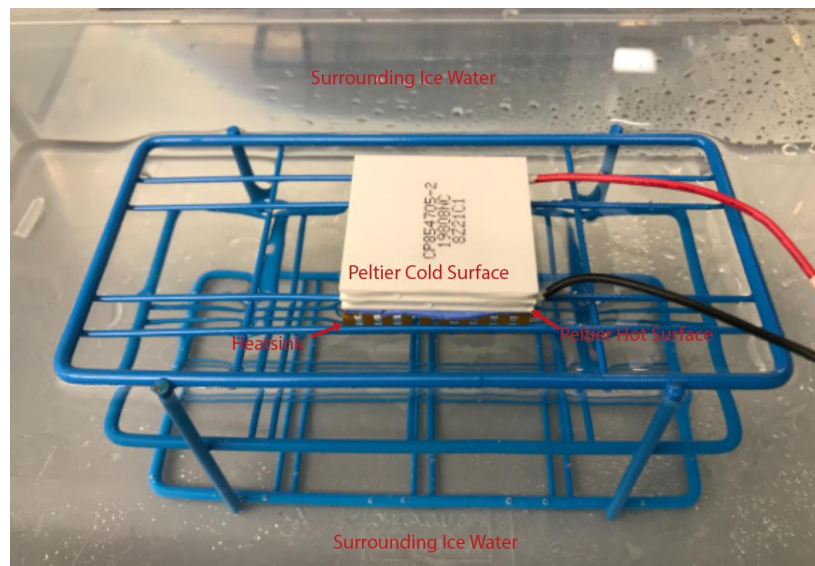


**Figure 11 Immersed Peltier Heatsink to Ice Bath/Water**

For this setup (**Figure 11**), the volume of water can be regarded as an infinite cooling

source for the hot surface of the Peltier. Thus, the hot surface should be kept cool. Due to the difficulty of measuring the temperature of items inside ice water, we have not figured out a way to measure the temperature of the hot surface. However, it is not critical, because our primary concern is whether the cold surface of the Peltier could reach the temperature of  $-18\text{ }^{\circ}\text{C}$ , which makes our cooling stage work according to our thermal simulation.

We used an infrared thermometer (SURPEER IR5D Laser Thermometer Gun) to measure the Peltier cold surface temperature. The reading was  $-20\text{ }^{\circ}\text{C}$  after 2 minutes and kept steady after we input the Peltier with  $12.2\text{V}$  voltage and  $4.94\text{A}$  current.

Similarly, we also tried to use thermal paste to attach the hot surface of the Peltier to a large aluminum block (**Figure 12**) and regarded this large aluminum block as a cooler for the Peltier. With inputting  $12\text{V}$  voltage and subsequently  $5.3\text{A}$  current, the cold surface reached  $-34.4\text{ }^{\circ}\text{C}$  after only 2 minutes and stabilized in this temperature. After 10 minutes, the large aluminum block area near to the Peltier has rose to  $23.7\text{ }^{\circ}\text{C}$ , only slightly above the room temperature  $20\text{ }^{\circ}\text{C}$ . (**Figure 12**)

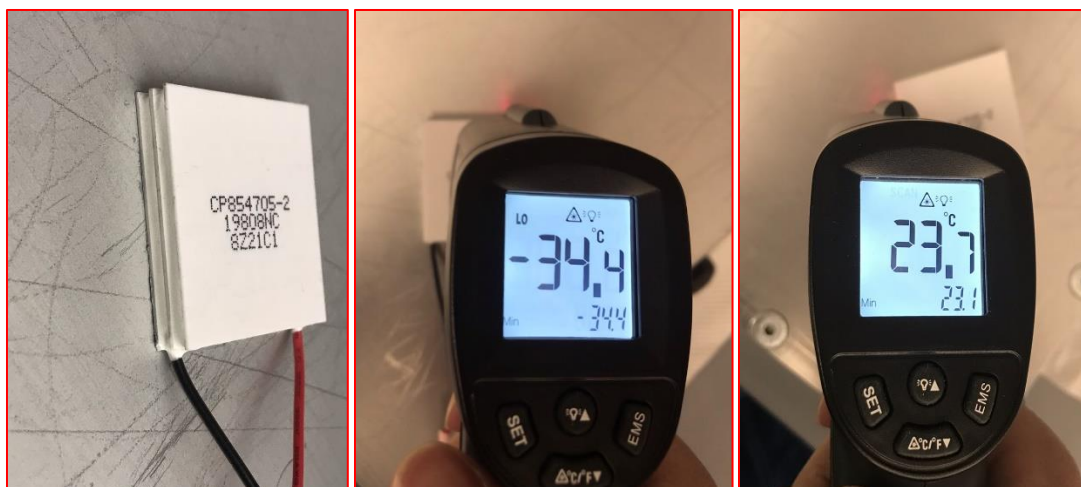


**Figure 12** With the hot surface of the Peltier pasted to large aluminum block, the cold surface reached  $-34.4\text{ }^{\circ}\text{C}$ , while the aluminum block reached only  $23.7\text{ }^{\circ}\text{C}$

With these two experiments, we confirm that our multi-stage Peltier could reach the

desired temperature if we can efficiently remove the heat generated.

### 3.1.3 Cultivation Plate Cooling

The thermal simulation shows us that, when the sapphire window, which contacts the cultivation plate directly, reaches an average temperature of  $-5\text{ }^{\circ}\text{C}$ , the agar inside the plate could reach between  $2\text{ }^{\circ}\text{C}$  –  $4\text{ }^{\circ}\text{C}$ . Under this temperature range, *C. elegans* can be immobilized wholly for proper imaging [42].

We immersed the heatsink on the hot surface of the Peltier to room temperature water, and adjusted the current so that the Peltier cold surface stabilized at  $-5\text{ }^{\circ}\text{C}$ . Now, this Peltier can be treated as the sapphire window in the thermal simulation.

We placed the cultivation plate with *C. elegans* culturing inside to the Peltier cold surface, while measuring the temperature of its agar using the same infrared thermometer (Figure 13).

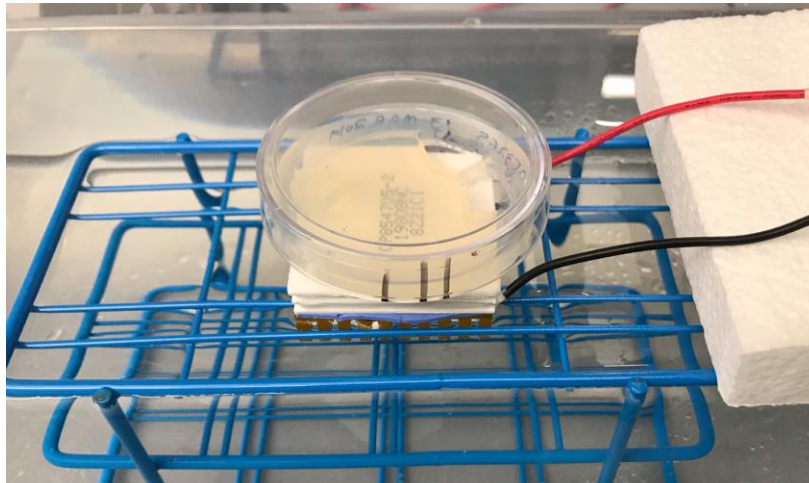


**Figure 13 Placement of Cultivation Plate on the Peltier**

After approximately 12 minutes, the agar inside of cultivation plate stabilized at  $4\text{ }^{\circ}\text{C}$  (Figure 14).



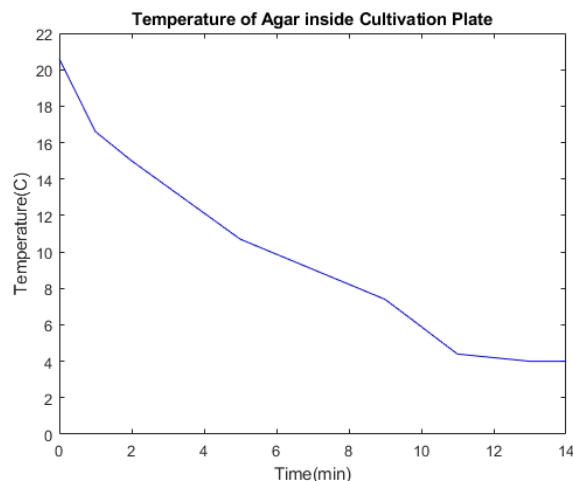


**Figure 14 Temperature of Agar inside Cultivation Plate**

We did not observe the agar reaching the lower simulated range of 2 °C, but only the upper simulated range of 4 °C. The main reason should be that the area of the cultivation plate is larger than the square surface of the Peltier. The diameter of the plate is 60 mm, while the dimension of the Peltier is 40 x 40 x 7.05 mm. Since a portion of the plate bottom area was still exposed to room temperature air, the temperature of the agar inside plate should be higher than if the plate's base area was fully contacting with the cold Peltier surface.

If the plate's entire bottom surface is in contact with the sapphire window, which is 80mm in diameter and -5 °C, we expect that the agar inside of cultivation plate will reach temperature lower than 4 °C, which is adequate to immobilize worms on the plate.

### **3.2 Active Illumination Microscopy (AIM) Initial Experiments**

To perform the wide-field AIM, the following procedure should be executed.

1. Take a large area image of the whole plate
2. Computer identifies and locates worms on agar

3. Computer identifies the nose and tail of the worm
4. Take multiple images of the worm nose, with different excitation light intensities
5. Base on images of different excitation intensity, use segmentation algorithm based on neuron fluorescence responsivity to do a coarse segmentation of the image
6. Input the segmented image to SLM
7. Shape the excitation light using the SLM.
8. AIM and improved image contrast achieved.

Based these procedures, we completed some initial experiments.

### 3.2.1 Worm Identification

There are many methods available for worm identification. Wormscan is a low-resolution method, which deals with large numbers of worms on cultivation plate, primarily used for worm counting [22, 23]. MindControl is a powerful tool written in C programming language using the open-source OpenCV computer vision library. This software is capable of conducting single worm identification and movement tracking [25], but it is not designed for multiple worms. Massive efforts need to be devoted to its modification for our identification task. WorMachine [24] is a three-step MATLAB-based image analysis graphical user interface (GUI) software and allows for (1) automated identification of *C. elegans* worms, (2) extraction of morphological features and quantification of fluorescent signals, and (3) machine learning techniques for high-level analysis (**Figure 15**).

Due to its capabilities, we chose WorMachine as our worm identification software. Then, we need to repeat the processing procedure in their paper to see whether their software fulfills our needs.

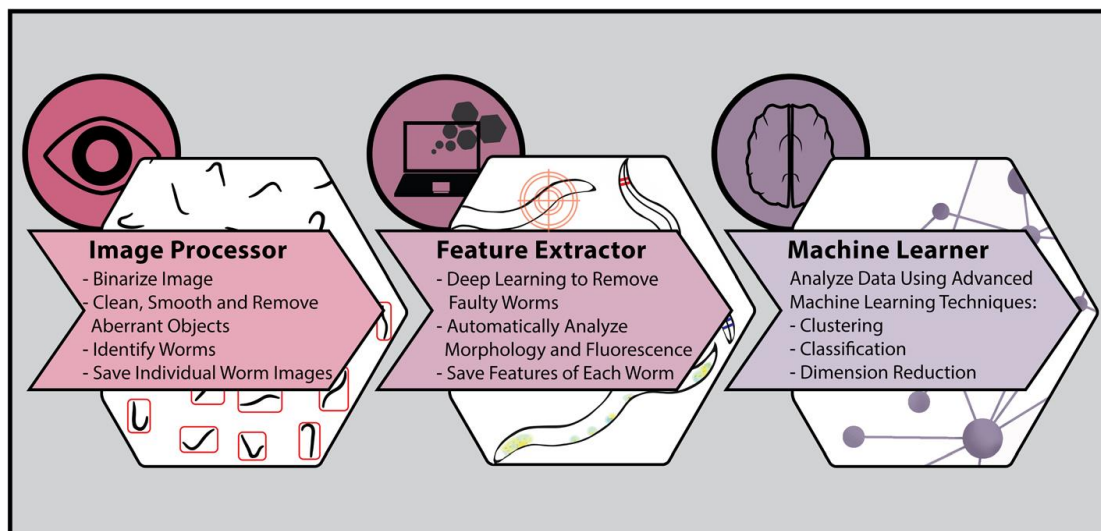


**Figure 15 WorMachine workflow. The software includes three main functions [24]**

The WorMachine papers mentioned that, for a better worm to background contrast, we should image worms on cultivation plates rather than slides [24, 48], which typically have lower contrast. This is advantageous because our goal is to use cultivation plates for imaging and laser surgery.

Worms are crawling on the agar before we immobilize them, so trails are always left behind them on their cultivation bacterial lawn [49] as observed in **Figure 16**. It is hard for most existing algorithms to tell the difference between trails and worms. Over exposing the camera (can be achieved by longer exposure time or higher illumination intensity) reduces visible trails in the image, while maintaining a reasonable worm to background ratio. In practice, a high enough illumination intensity might not be easily achievable, thus we use a longer exposure time to obtain the over exposure.

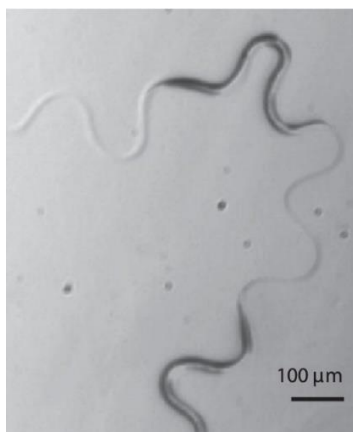


**Figure 16 *C. elegans* and its Trails on Agar [50]**

To ensure a clearer image throughout a longer exposure time, worms must be immobilized. We did not use M9 and sodium azide for immobilization as stated in the WorMachine paper, because we already have the alternative method for immobilization – cold temperature. It was easy for us to cool cultivation plates to 4 °C in refrigerator.

They also mentioned that, if worms are in a full circle, such as when one of their ends contact with some other point on their body, they cannot be identified with their software and will be marked as faulty. Also, worms touching another worm or other objects directly can cause WorMachine to fail. So, it is better to separate touching worms on the plate before taking images on a microscope.

We used our Leica M205 FA with 1X objective to acquire a large image of the plate. We first counted the number of worms manually for reference, and we counted only those worms that are not touching the boundary of the FOV, following what the WorMachine paper said. The number we counted was 18, and we manually marked them in **Figure 17**.

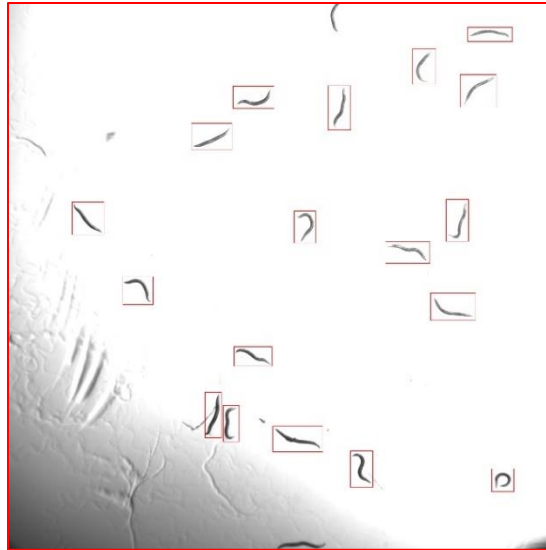


**Figure 17 Large Image of Worms on An Unseeded Agar Plate, the quantity was 18**

Then, we inputted the large image to the WorMachine and tried to identify worms. The WorMachine was able to recognize all those 18 targeted worms. However, as stated in both WorMachine paper and Leifer's paper [25], some trails or tracks on agar can be counted as a worm, so WorMachine counted 19 worms, mistakenly identifying a short track as a worm (Figure 18).

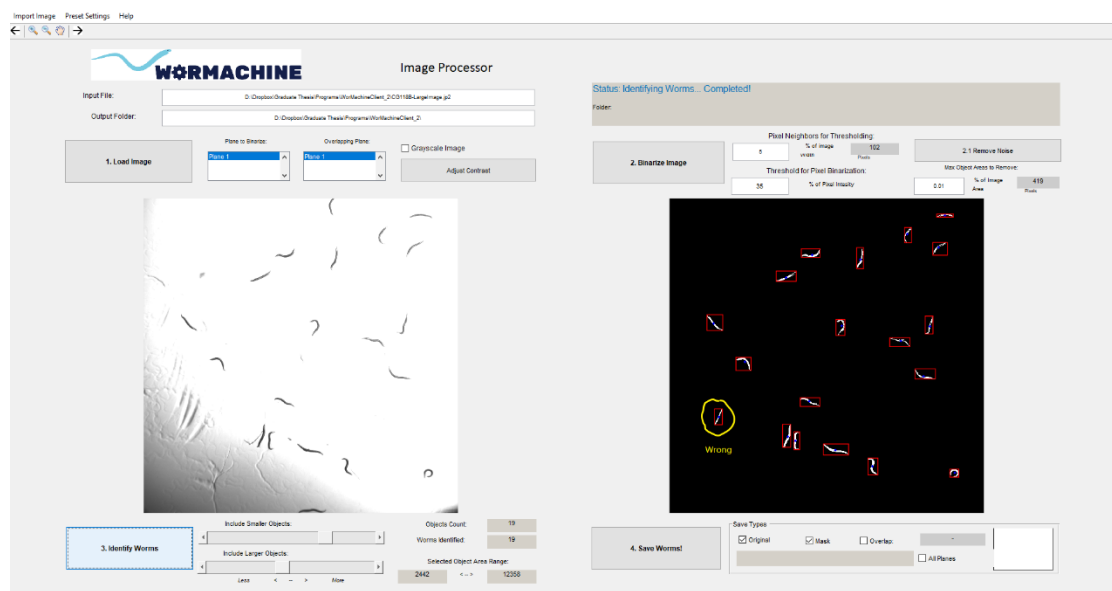


**Figure 18 Worm Identification using ImageProcessor in WorMachine, with a Track on Agar Incorrectly Identified as a Worm.**

WorMachine has the function to delete an incorrectly marked worm afterward manually. So, it is not too troublesome to have a few incorrectly identified worms. Nevertheless, algorithm improvement for WorMachine is preferred in the future.

After the worm identification, we still need to mark each worm's nose and tail. WorMachine provides another function called Features Extractor. We tested this function with some existing identified worms by the previous ImageProcessor in WorMachine. The ImageProcessor worked well, with high accuracy of identifying noses and tails of worms (Figure 19).

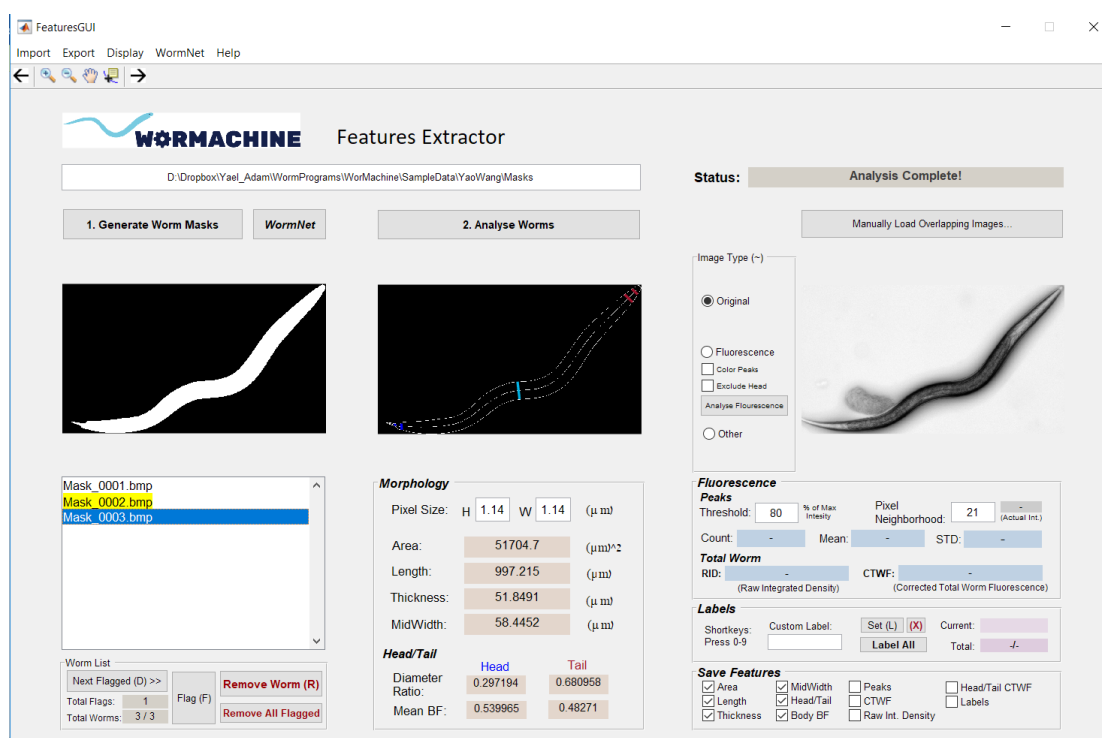


**Figure 19 The Features Extractor in WorMachine Successfully Identified the Nose and the Tail of a Worm in Our Experiment**

One function we'd like to add to WorMachine is to the ability to export the coordinates of each worm's nose. Only with the coordinates of the nose will we be able to precisely move our microscope stage to that specific location and change to higher magnification for further imaging, processing, and laser surgery. As we utilize the GUI more and more in

Matlab, we expect to complete this goal on our own shortly.

### 3.2.2 Slit Image

In Goal 2, we plan to use a transmissive SLM for patterning the illumination when placing the SLM into our microscope field stop, a conjugate plane to the sample plane.

Transmissive SLM is based on a transmissive Liquid Crystal (LC) microdisplay with  $L \times W$  (e.g. 1024 x 768) pixel resolution. Every pixel is controlled by circuit independently to block light by a certain degree. Thus, when light comes through a transmissive SLM, its spatial distribution can be patterned accordingly to the grayscale of all SLM's pixels. For example, if we input a SLM with a total black image and then shine a light through the SLM, an entirely black image will appear on the image plane, meaning no light comes through. If we draw a white line on the inputted black image, we will illuminate a line on the image plane.

Since we did not possess an SLM, we imitated it by creating a slit on a sheet of aluminum foil. We use a slit on a sheet of aluminum foil to imitate a transmissive SLM. The slit on foil represented the white line on the black image.

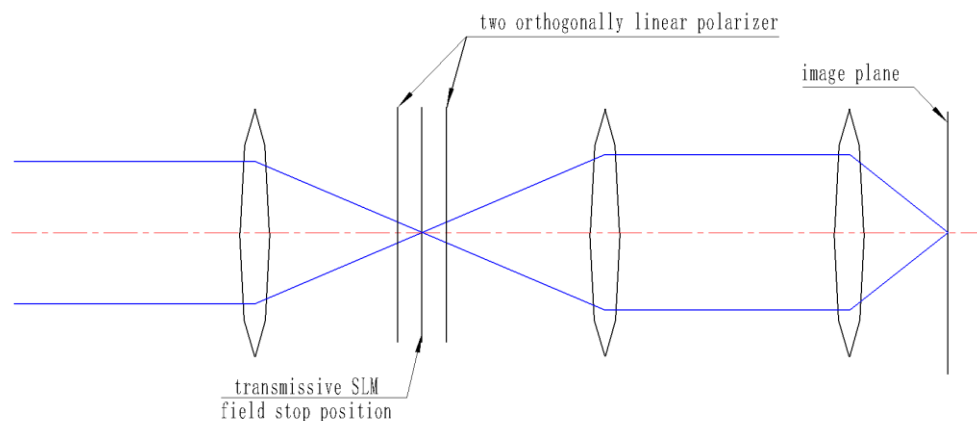


**Figure 20 Beam-path of using SLM to pattern light**

We placed a sheet of aluminum foil with a 30- $\mu\text{m}$  width slit into the field stop position of our microscope and excited a film of evaporated gelatin conjugated with Oregon Green

dye (ThermoFisher) on the microscope sample plane. We used a 30  $\mu\text{m}$  width slit because the pixel pitch of a typical transmissive SLM is 36  $\mu\text{m}$ , thus this slit is close to the smallest slit image a transmissive SLM could provide. We wanted to know whether the resolution of this patterning is sufficient for our imaging application, which has the smallest detail that is roughly 1  $\mu\text{m}$  in width.

The image of the Oregon Green dye on the sample plane shows that the linear illumination has a resolution of 0.55  $\mu\text{m}$ . Because the smallest detail that we image is roughly 1  $\mu\text{m}$  in width, we expect that the hardware developed in goal 2 will pattern the illumination with resolution sufficient for our imaging application.

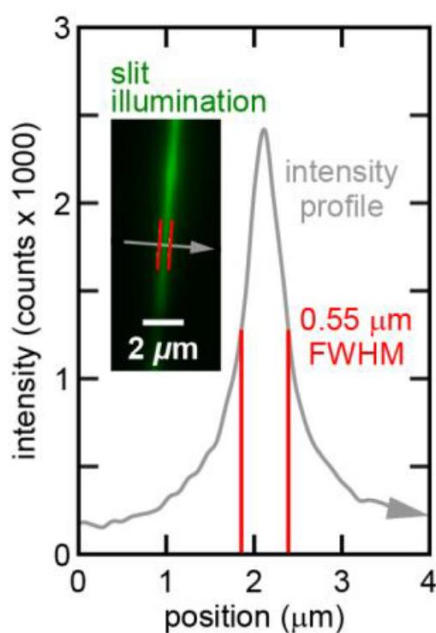


**Figure 21 Slit patterned illumination with 0.55  $\mu\text{m}$  resolution. Thin slit at field stop illuminates dye through 1.4 NA, 60x objective. Plot shows intensity along the gray line**

We also measured the contrast between the patterned illumination peak and dark background 2  $\mu\text{m}$  away from the slit, and the ratio is 23/1 on average. This means that we may achieve an SBR that is close to 14 dB, using our SLM setup, when inputting a binary image to the SLM if the SLM pixels can be completely white or black.



### 3.2.3 Microscope Patterned Illumination using SLM LC2002

There are two transmissive SLM candidates for the light patterning, Holoeye LC 2012 and Holoeye LC 2002. A comparison between these two is list below in Table 3.

**Table 3 Comparison between LC2012 and LC2002**

	LC 2012	LC 2002
Display Type:	Transmissive LC	Transmissive LC
Resolution:	1024 x 768	800 x 600
Pixel Pitch:	36 $\mu\text{m}$	32 $\mu\text{m}$
Fill Factor:	0.58	0.55
Display dimension	50x56x5.4mm	40 x38 x5.4mm
Active Area	36.9 x 27.6 mm	21,0 x 26,0 mm
Addressing	8 Bit (256 Grey Levels)	8 Bit (256 Grey Levels)
Signal Formats	HDMI – XGA Resolution	VGA – SVGA Resolution
Input Frame Rate	60 Hz	60 Hz

From the comparison, even though LC2012 is a newer model, it has a larger pixel pitch, which will reduce the resolution of patterned illumination. Also, the dimension of the LC2012 display is 50 x 56 x 5.4mm, which is bigger than the mouth dimension (39 x 14 mm) of our microscope field stop, making it hard to be implanted into the field stop. Those two reasons made us choose the LC2002 transmissive SLM for future embedding to Ti2 microscope.

Still, without several hardware modifications, it is not possible to put both polarizers and LC2002 display into the field stop. Thus, we had to mimic the illumination and its patterning outside of the microscope. We designed the following beam path for real

experiment (**Figure 22**).

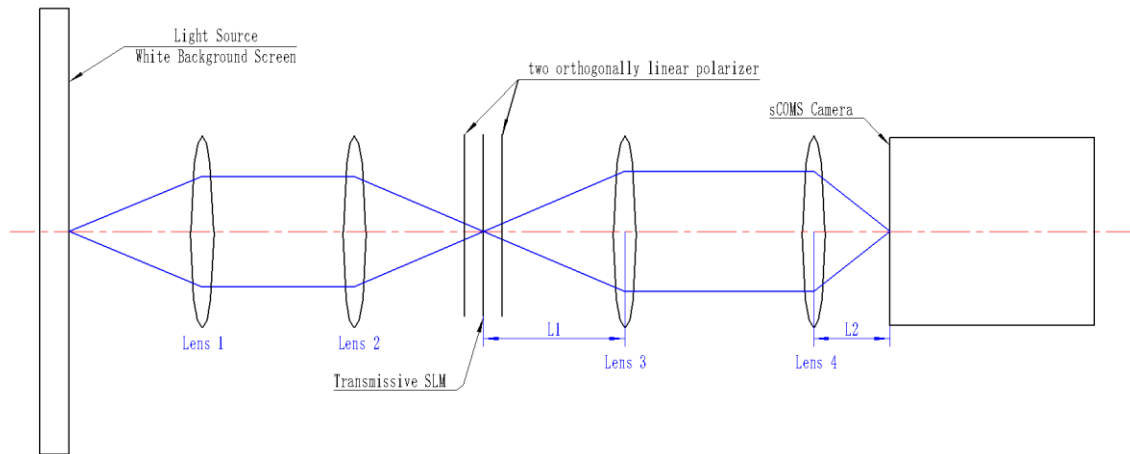


**Figure 22 Beam Path Scheme for Real Illumination Patterning**

When showing a white image on the screen, a cellphone acts as a plane light source, similar to the LED illumination source (Nikon SOLA SE II) we are using for Nikon Ti2 microscope. The difference between the cellphone screen and the Nikon LED illumination source are: 1. The brightness of the cellphone screen is much lower; 2. Area of the screen is much bigger. Despite these differences, the functionality remains the same.

Changing the focal length  $L1$  and  $L2$  in **Figure 22**, or saying, changing to different lens 3 and lens 4 will result in the shape showing on SLM to stretch by a factor of  $L2/L1$  onto the camera image plane. For example, if the SLM shows a 10 mm length of a white line, and  $L1=50$  mm,  $L2=100$  mm, then there will be a line shape showing in the camera imaging plane with a length of  $10 \times (100/50) = 20$  mm, which is magnified by a factor of 2. Similarly, if we use  $L1=100$  mm and  $L2=50$  mm, there will be a line shape showing in the camera plane with a length of  $10 \times (50/100) = 5$  mm, which is shrunk by a factor of 2.

In a microscope, the values of  $L1$  and  $L2$  are determined by dimensions of the field stop iris, the sample plane field of view (FOV) and the lenses inside. The shape forming

on the SLM will shrink by a factor of  $L2/L1$  and then shine to the sample.

For now, we only need to know whether the SLM can pattern the illumination to a desired shape. Thus, a sample is not needed. Instead, we put an sCMOS camera at the sample plane. For this setup (**Figure 23**), the shape that we will see on the camera will be the illumination shape projected onto the sample plane.

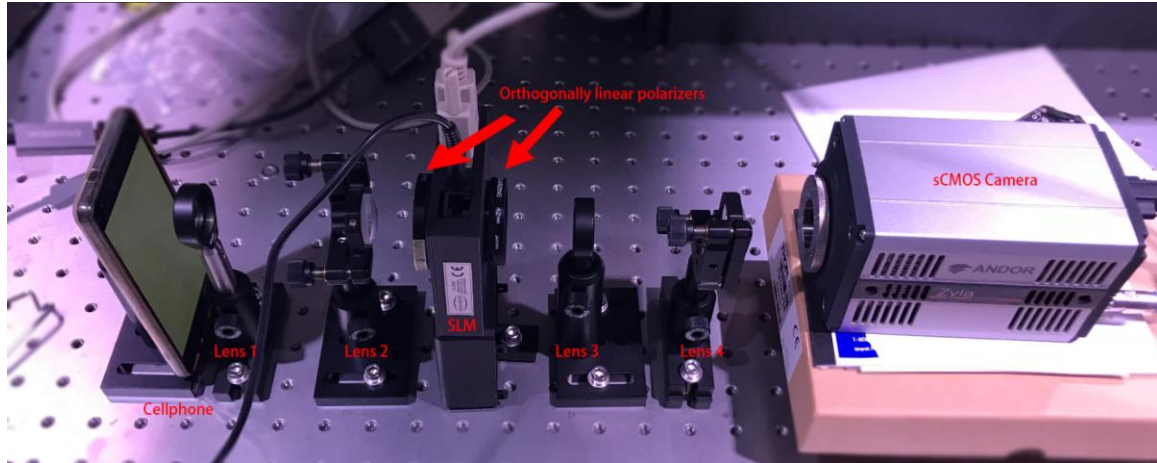


**Figure 23 Real Illumination Patterning Setup**

**Figure 24 (a)** shows the pattern we inputted to the SLM, and **Figure 24 (b)** shows the picture we saw on the camera.

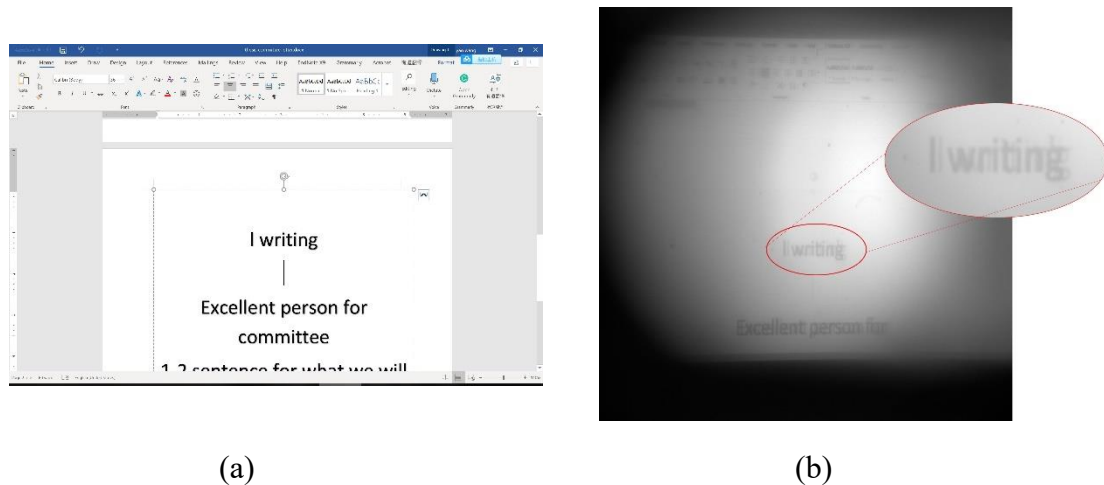


**Figure 24 SLM Input Image and Camera Output Image. There is a blurry ghost image in (b) due to SLM LC2002 damage.**

The output image is still not as defined as we anticipated. However, considering this

is only an unrefined setup that was constructed outside of the microscope, which does not possess a perfect beam path alignment as it would inside a microscope, it nonetheless provides a decent result and demonstrates the feasibility to pattern the light to an arbitrary shape with our microscope setup.

### 3.2.4 Neuron Coarse Segmentation

To pattern the illumination light to a desired shape, the SLM needs an input image. This image is a coarsely segmented image derived from our neuron responsivity algorithm.

In our planned setup, we will use multi-intensity point scanning to analyze every pixel's responsivity. However, without the insertion of an SLM into our wide-field microscope, we cannot do the scanning. Even so, we can test our algorithm on wide-field images, to see whether it is good at the segmentation of neurons.

A *ptrx-1::trx-1::gfp* transgene in our *C. elegans* strain leads to expression of thioredoxin, a natural redox protein found in the worm, fused to green fluorescent protein (GFP). This particular protein is localized to the ASJ neuron throughout its cell body, dendrites, and axons. Therefore, the ASJ neuron contains GFP while the background tissue does not. Because the neuron contains GFP, its emission intensity is dependent on the illumination intensity. For other tissue that contains no GFP, the brightness comes mostly from scattered light, which is less dependent on the illumination intensity at that pixel. Probing tissue “responsivity” pixel-by-pixel will allow us to ascertain if the pixel's light originates directly from the neuron or scattering.

Derived from this theory, if we illuminate the whole sample with three different illumination  $I^{\text{in}}$ , and then check every pixel's emission intensities  $I^{\text{out}}$ , we expect that a neuron pixel's  $I^{\text{out}}$  is more steeply dependent on its  $I^{\text{in}}$  than a background tissue pixel does. Thresholding this ‘steepness’ will give us a segmentation of neuron and other tissues.

We define a fluorescence responsivity index (RI) =  $R_{\text{high}} / R_{\text{low}} = (I_{\text{high}}^{\text{out}} / I_{\text{high}}^{\text{in}}) / (I_{\text{low}}^{\text{out}} / I_{\text{low}}^{\text{in}})$  here. We will test whether using only this RI can segment an image properly.

In our algorithm, when taking three different illumination intensity (low, medium, high) of images, we treat one pixel's RI as a ratio,

$$\text{Ratio} = ((I_{\text{medium}}^{\text{out}} / I_{\text{low}}^{\text{out}}) / (I_{\text{medium}}^{\text{in}} / I_{\text{low}}^{\text{in}})) * ((I_{\text{high}}^{\text{out}} / I_{\text{low}}^{\text{out}}) / (I_{\text{high}}^{\text{in}} / I_{\text{low}}^{\text{in}})) \quad \text{Eq. 3-1}$$

According to our tissue responsivity theory, if a pixel contains a neuron with GFP, the Ratio should be close to 1 or even higher; but if a pixel does not contain a neuron, we should see less difference between  $I_{\text{high}}^{\text{out}}, I_{\text{medium}}^{\text{out}}$  and  $I_{\text{low}}^{\text{out}}$ , thus, the Ratio should be relatively close to

$$\text{Ratio} = (1 / (I_{\text{medium}}^{\text{in}} / I_{\text{low}}^{\text{in}})) * (1 / (I_{\text{high}}^{\text{in}} / I_{\text{low}}^{\text{in}})) \quad \text{Eq. 3-2}$$

As mentioned in chapter 2.2, to differentiate between a GFP and a non-GFP pixel, a lower  $I_{\text{low}}^{\text{in}} / I_{\text{high}}^{\text{in}}$  setup is preferred. Thus, we chose illumination intensity of 10%, 40%, and 80%, and used our automated image acquiring macro (see Appendix, 6.1) in Nikon NIS-Elements (Nikon's microscope controlling software) to acquire those images. Using this macro accelerates the image acquiring speed tremendously and thus helps to prevent the negative impact and responsivity inaccuracy caused by photobleaching.

We took three wide-field images on the same location of a *daf-11(sa195); ptrx-1::trx-1::gfp* strain *C. elegans* (**Figure 25**). This strain is a GFP labeled and has the brightest GFP expression in our lab. It is easier to test our algorithm on a brighter GFP labeled strain than a dimmer one.



**Figure 25** Images with 10%, 40% and 80% intensity in turn, on *C. elegans*' ASJ neuron. All images are in 16-bit depth, with the same contrast adjustment.

To confirm our theory, we first manually checked the Ratio map of several pixels of neuron, cell body, and background tissues, computed from three images took on three different illumination intensity. For background, we examined pixels close to the neuron and pixels far from the neuron.

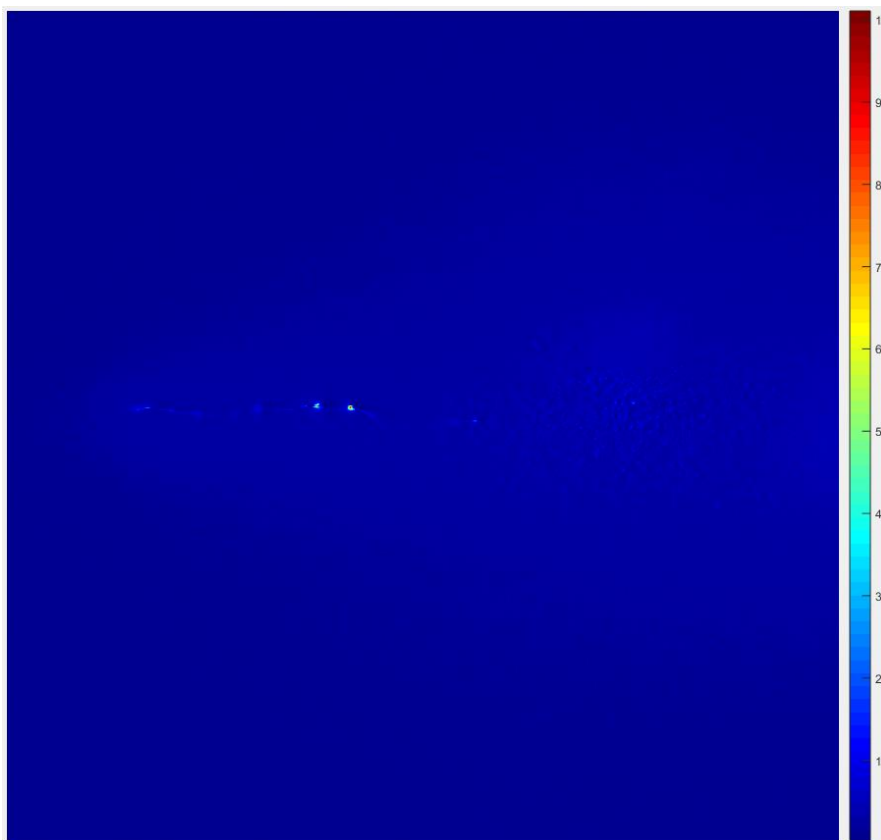


**Figure 26** Ratio Heatmap Calculated from the Images Set

From **Figure 26**, we can effortlessly see the Ratio difference between neuron, cell body, and background. This gives us an opportunity to use a threshold to segment neuron from images.

The core part of Ratio thresholding script is printed below (code with Matlab 2018b).

```

%% Get new images after dividing by a factor
I1new=I1./1; % 10% intensity means dividing factor 1
I2new=I2./4; % 40% intensity means dividing factor 4
I3new=I3./8; % 80% intensity means dividing factor 8

IRatio=(I2new./I1new).*(I3new./I1new); % Same equation to Eq. 3-1
IFinal=IRatio;

MeanOfIFinal=mean(mean(IFinal)); % threshold will rely on this mean

Locate1=find(IRatio>3*MeanOfIFinal); % find elements that are larger
than a ratio. This is an important threshold, we need to find a better
way to define it in the future
IFinal(Locate1)=[1]; % set all elements larger than a ratio of to 1
Locate2=find(IRatio<3*MeanOfIFinal); % find elements that are smaller
than a ratio
IFinal(Locate2)=[0]; % set all elements smaller than a ratio of to 0
imshow(IFinal,[])

```

This is a binary segmentation using the threshold. We defined the threshold here by adjusting it to acquire the best performance. For this set of images, it gave a reasonable result of segmentation (**Figure 27**).



**Figure 27 Segmented Image Using the Above Images Set**

However, using the same threshold on other image sets may not always produce an acceptable result. This result means that some other threshold related parameters need to be considered, not only the mean of all the Ratio of images.

Prior to determining new parameters to define an appropriate threshold, we will first need to install the SLM to our wide-field microscope, so we can scan through the sample, instead of using stray illumination while receiving emission light from everywhere in the sample. With illumination scanning using SLM and receiving light only from those scanning pixels, we can be more confident in whether our responsivity segmentation algorithm works well for our future AIM purpose.



## 4. SUMMARY

Our high-throughput microscopy platform is a long-term project; thus, we will complete the planned setup in the future. Therefore, as declared in this paper title, we are assessing the feasibility of achieving the final goals with our planned setup in this paper.

We divided our final goal of high-throughput microscopy platform into two specific goals: cooling stage and AIM. To verify whether the cooling stage is achievable and whether the stage could immobilize worms as predicted, we did three initial experiments: 1. The thermal simulation shows us that, within a normal multi-stage Peltier's cooling capability and using typical materials, the heat in a cultivation plate can be removed by the cold surface of the Peltier, and the agar temperature can drop to 2 - 4 °C, which is proper for immobilization of *C. elegans*; 2. The Peltier testing confirms that the selected multi-stage Peltier can reach a much better (-34 °C) temperature than the temperature calculated from the thermal simulation (-18 °C), which gives us more abundant cooling power source for use in the real setup; 3. The cultivation plate cooling test is meaningful because it predicts the sapphire window's ability to cool the cultivation plate. Directly testing the thermal conduction between the cultivation plate and its plane of contact eliminates many other unrelated factors; thus the result is more convincing. From the thermal simulation, when the sapphire window reaches -5 °C, the agar will reach the desired temperature. The preliminary experiments confirmed the simulated result, making the cooling stage more promising.

To demonstrate the achievability of AIM, we completed four initial experiments: 1.

Worm identification shows that an existing method already can identify worms and distinguish their noses and tails. However, we still need much effort to implant the WorMachine's function into our working procedure, while adding some new functions, such as a function that can export worm coordinates to the microscope stage. 2. The slit image shows how sharp the patterning illumination on the sample plane can be if we put a transmissive SLM into our field stop. As the sharpness of illumination already exceeded the finest detail of *C. elegans* we need to image, we believe that patterned light can illuminate on only the axons and dendrites of a neuron. 3. The experiment for microscope patterned illumination using SLM LC2002 mimics the beam path inside our inverted microscope. It illustrates that it is possible to pattern illumination to an arbitrary shape by installing transmissive SLM in the field stop position. 4. The neuron coarse segmentation algorithm we introduced was able to complete neuron segmentation with high speed. Even though this algorithm did not work great on every image set, we can further perfect it, not mentioning that we have not given the algorithm its optimum applying images – images attained by point scanning microscopy. We believe that, with a SLM being installed to our microscope and obtaining scanning images, the algorithm will have much better performance.

As described in Appendix, besides the cooling stage and AIM, we also made some important progress to ensure that we could reach our goals. Those macros we wrote are very flexible in doing complicated jobs and easy to be transplanted to other software, like Matlab. It means that we are realizing functions for our Matlab based App for future AIM. The Nikon SDK experiment helps us attain experience in controlling multiple devices within one software (Matlab). With carefully designing functions in future App, we will be able to process our high-throughput microscope platform efficiently.

In summary, in this paper, we first introduced our long-term project – high throughput microscopy platform, i.e. automated laser surgery. We explained how we can make the laser surgery automated, and why the automation is so important for both our lab and many other neuroscience labs that use *C. elegans* model. Then, we stated our detailed plan on the whole setup to achieve the final laser surgery automation goal. This is still a big picture of what we should achieve for the final goal, but it shows the direction we should take our research. Then, we ran several initial experiments to support our proposal to advance our ability to create a high throughput microscopy platform for neuroscience research in *C. elegans*. With the completion of those experiments, we conclude that it is feasible to achieve our Goal 1, reduced preparing time, and Goal 2, improve image contrast, which are critical pathways to our final high throughput microscopy platform.

## 5. REFERENCE

1. Shin, J.E., et al., *Dual leucine zipper kinase is required for retrograde injury signaling and axonal regeneration*. Neuron, 2012. **74**(6): p. 1015-1022.
2. Hoffman, P.N., *A conditioning lesion induces changes in gene expression and axonal transport that enhance regeneration by increasing the intrinsic growth state of axons*. Experimental neurology, 2010. **223**(1): p. 11-18.
3. McQuarrie, I.G. and B. Grafstein, *Axon outgrowth enhanced by a previous nerve injury*. Archives of neurology, 1973. **29**(1): p. 53-55.
4. Flohr, H. and W. Precht, *Lesion-induced neuronal plasticity in sensorimotor systems*. 2013: Springer Science & Business Media.
5. Richardson, P. and V. Issa, *Peripheral injury enhances central regeneration of primary sensory neurones*. Nature, 1984. **309**(5971): p. 791.
6. Neumann, S. and C.J. Woolf, *Regeneration of dorsal column fibers into and beyond the lesion site following adult spinal cord injury*. Neuron, 1999. **23**(1): p. 83-91.
7. Chung, S.H., et al., *Novel DLK-independent neuronal regeneration in *Caenorhabditis elegans* shares links with activity-dependent ectopic outgrowth*. Proc Natl Acad Sci U S A, 2016. **113**(20): p. E2852-60.
8. Brenner, S., *The genetics of *Caenorhabditis elegans**. Genetics, 1974. **77**(1): p. 71-94.
9. *Genome Sequence of the Nematode *C. elegans*: A Platform for Investigating Biology*. Science, 1998. **282**(5396): p. 2012-2018.

10. Chung, S.H., et al., *The role of the AFD neuron in C. elegans thermotaxis analyzed using femtosecond laser ablation*. BMC Neurosci, 2006. **7**: p. 30.
11. Chung, S.H. and E. Mazur, *Femtosecond laser ablation of neurons in C. elegans for behavioral studies*. Applied Physics A, 2009. **96**(2): p. 335-341.
12. Kutscher, L.M. and S. Shaham, *Forward and reverse mutagenesis in C. elegans*. WormBook: the online review of C. elegans biology, 2014: p. 1.
13. Chu, K.K., D. Lim, and J. Mertz, *Practical implementation of log-scale active illumination microscopy*. Biomedical optics express, 2010. **1**(1): p. 236-245.
14. Bargmann, C.I. and L. Avery, *Laser killing of cells in Caenorhabditis elegans*, in *Methods in cell biology*. 1995, Elsevier. p. 225-250.
15. Rohde, C.B., et al., *Microfluidic system for on-chip high-throughput whole-animal sorting and screening at subcellular resolution*. Proceedings of the National Academy of Sciences, 2007. **104**(35): p. 13891-13895.
16. Hulme, S.E., et al., *A microfabricated array of clamps for immobilizing and imaging C. elegans*. Lab on a Chip, 2007. **7**(11): p. 1515-1523.
17. Chung, K., M.M. Crane, and H. Lu, *Automated on-chip rapid microscopy, phenotyping and sorting of C. elegans*. Nature methods, 2008. **5**(7): p. 637.
18. Rohde, C.B. and M.F. Yanik, *Subcellular in vivo time-lapse imaging and optical manipulation of Caenorhabditis elegans in standard multiwell plates*. Nat Commun, 2011. **2**: p. 271.
19. Pawley, J., *Handbook of biological confocal microscopy*. 2010: Springer Science & Business Media.
20. Denk, W., Strickler, J. H., & Webb, W. W., *Two-photon laser scanning fluorescence microscopy*. Science, 1990.

21. Wilson, T., *Confocal microscopy*. Vol. 426. 1990: Academic press London.
22. Puckering, T., et al., *Automated Wormscan*. F1000Res, 2017. **6**: p. 192.
23. Mathew, M.D., N.D. Mathew, and P.R. Ebert, *WormScan: a technique for high-throughput phenotypic analysis of Caenorhabditis elegans*. PLoS One, 2012. **7**(3): p. e33483.
24. Hakim, A., et al., *WorMachine: machine learning-based phenotypic analysis tool for worms*. BMC Biol, 2018. **16**(1): p. 8.
25. Leifer, A.M., et al., *Optogenetic manipulation of neural activity in freely moving Caenorhabditis elegans*. Nat Methods, 2011. **8**(2): p. 147-52.
26. Gala, R., et al., *Active learning of neuron morphology for accurate automated tracing of neurites*. Front Neuroanat, 2014. **8**: p. 37.
27. Zhou, Z., et al., *TReMAP: Automatic 3D Neuron Reconstruction Based on Tracing, Reverse Mapping and Assembling of 2D Projections*. Neuroinformatics, 2016. **14**(1): p. 41-50.
28. Qu, L., F. Long, and H. Peng, *3-D Registration of Biological Images and Models: Registration of microscopic images and its uses in segmentation and annotation*. IEEE Signal Processing Magazine, 2015. **32**(1): p. 70-77.
29. Mukherjee, S., B. Condrón, and S.T.J.I.T.o.I.P. Acton, *Tubularity flow field—a technique for automatic neuron segmentation*. 2015. **24**(1): p. 374-389.
30. Uzunbaş, M.G., C. Chen, and D. Metaxas. *Optree: a learning-based adaptive watershed algorithm for neuron segmentation*. in *International Conference on Medical Image Computing and Computer-Assisted Intervention*. 2014. Springer.
31. Uzunbas, M.G., C. Chen, and D.J.M.i.a. Metaxas, *An efficient conditional random field approach for automatic and interactive neuron segmentation*. 2016. **27**: p. 31-44.
32. Basu, S., et al. *Tree2Tree: neuron segmentation for generation of neuronal morphology*. in *ISBI*. 2010. Citeseer.

33. Chen, T., K.-K. Ma, and L.-H. Chen, *Tri-state median filter for image denoising*. IEEE Transactions on Image processing, 1999. **8**(12): p. 1834-1838.
34. Boulanger, J., et al., *Patch-based nonlocal functional for denoising fluorescence microscopy image sequences*. IEEE transactions on medical imaging, 2010. **29**(2): p. 442-454.
35. Soulez, F., et al. *Blind deconvolution of 3D data in wide field fluorescence microscopy*. in *2012 9th IEEE International Symposium on Biomedical Imaging (ISBI)*. 2012. IEEE.
36. Kim, B. and T. Naemura, *Blind depth-variant deconvolution of 3D data in wide-field fluorescence microscopy*. Scientific reports, 2015. **5**: p. 9894.
37. Rivenson, Y., et al. *Deep Learning Microscopy: Enhancing Resolution, Field-of-View and Depth-of-Field of Optical Microscopy Images Using Neural Networks*. in *CLEO: Applications and Technology*. 2018. Optical Society of America.
38. Xue, Y., et al., *Scanless volumetric imaging by selective access multifocal multiphoton microscopy*. Optica, 2019. **6**(1): p. 76-83.
39. Yang, R., et al., *Neuronal imaging with ultrahigh dynamic range multiphoton microscopy*. Sci Rep, 2017. **7**(1): p. 5817.
40. Caarls, W., et al., *Minimizing light exposure with the programmable array microscope*. J Microsc, 2011. **241**(1): p. 101-10.
41. Schaffer, C.B., A. Brodeur, and E. Mazur, *Laser-induced breakdown and damage in bulk transparent materials induced by tightly focused femtosecond laser pulses*. Measurement Science and Technology, 2001. **12**(11): p. 1784.
42. Robinson, J.D. and J.R. Powell, *Long-term recovery from acute cold shock in *Caenorhabditis elegans**. BMC Cell Biol, 2016. **17**: p. 2.

43. Snyder, G.J., et al. *Hot spot cooling using embedded thermoelectric coolers*. in *Twenty-Second Annual IEEE Semiconductor Thermal Measurement And Management Symposium*. 2006. IEEE.
44. Efron, U., *Spatial light modulator technology: materials, devices, and applications*. Vol. 47. 1994: CRC press.
45. Zhang, M., et al., *Experimental Determination of Thermal Conductivity of Water– Agar Gel at Different Concentrations and Temperatures*. *Journal of Chemical & Engineering Data*, 2010. **56**(4): p. 859-864.
46. Karimi, G., J. Culham, and V. Kazerouni, *Performance analysis of multi-stage thermoelectric coolers*. *international journal of refrigeration*, 2011. **34**(8): p. 2129-2135.
47. DiSalvo, F.J., *Thermoelectric cooling and power generation*. *Science*, 1999. **285**(5428): p. 703-706.
48. Moulden, B., F. Kingdom, and L.F. Gatley, *The standard deviation of luminance as a metric for contrast in random-dot images*. *Perception*, 1990. **19**(1): p. 79-101.
49. Nguyen, J.P., et al., *Automatically tracking neurons in a moving and deforming brain*. *PLoS Comput Biol*, 2017. **13**(5): p. e1005517.
50. Padmanabhan, V., et al., *Locomotion of C. elegans: a piecewise-harmonic curvature representation of nematode behavior*. *PloS one*, 2012. **7**(7): p. e40121.



## 6. APPENDIX

### 6.1 Macros in Nikon NIS-Elements

Native to the Nikon Ti2 inverted microscope, Nikon provided us a powerful microscope software called NIS-Elements. NIS-Elements combines powerful image acquisition, analysis, visualization and data sharing tools. It is a flexible software platform for controlling Nikon microscopes and microscope's 3rd-party components (like our Andor Zyla 5.5 sCMOS camera that was installed to this Ti2 microscope), with powerful custom programming tools for image acquisition and analysis.

With this software, we were able to create many useful macros which not only accelerates our imaging and laser surgery processes but also made some previously impossible procedures feasible.

Macros are written in C-base programming language, with the help of several packed functions wrote by Nikon's engineers. We can use macros to combine those functions together and achieve much more complicated functions.

We list some macros we code inside NIS-Elements in this paper to show what our macros can do, and why we need those macros for our automated laser surgery project.

#### 1. LiveFeedback

In our planned automated laser surgery scenario, after the computer algorithm had figured out the exact coordinates of the sample that the laser should shoot, the microscope stage will move that coordinate to the laser spot location (usually the laser spot location is fixed near to the center of FOV). In an ideal condition, the microscope stage will move the

sample to the surgery location precisely. However, in practice, many disadvantageous factors, like stage idle stroke and offset stage movement and *etc*, hamper this precise movement from happening.

If, after stage relocation, there is still a small offset from the desired location, we need to have a live feedback function to correct the stage displacement.

We wrote a simple but robust macro algorithm for this procedure. After the first stage movement, the algorithm will search in eight different directions within a defined radius, to see whether the original location has the highest intensity. If yes, the stage will keep still. If within the searched radius to a direction, there is a pixel that has the highest intensity, the stage will move along this direction to that bright pixel (**Figure 28**).

One parameter here is essential: the radius of searching. If we define a larger radius, the stage may move to some undesired location, which is brighter but not our aimed neuron. If we define a smaller radius, the macro induced stage movement may not compensate for the initial stage offset.

According to our microscope manipulation experience, the maximum initial stage offset is within 2  $\mu\text{m}$ . We are using a 60X objective, and the real size per pixel under this objective is 0.108  $\mu\text{m}$ . Therefore,  $2/0.108 = 18.5$  pixels is an adequate searching radius. However, considering some unforeseen outliers in the future, we defined the search radius as 30 pixels. Which means, our algorithm will search from the initial spot to respectively 30 pixels in eight directions and trying to find the brightest pixel.

To ensure the performance, our algorithm repeats a similar brightest spot searching, but with a smaller radius, usually 5 pixels, in four directions.

We tried this algorithm a few hundred times in different situations, and it worked with >95% accuracy at moment.

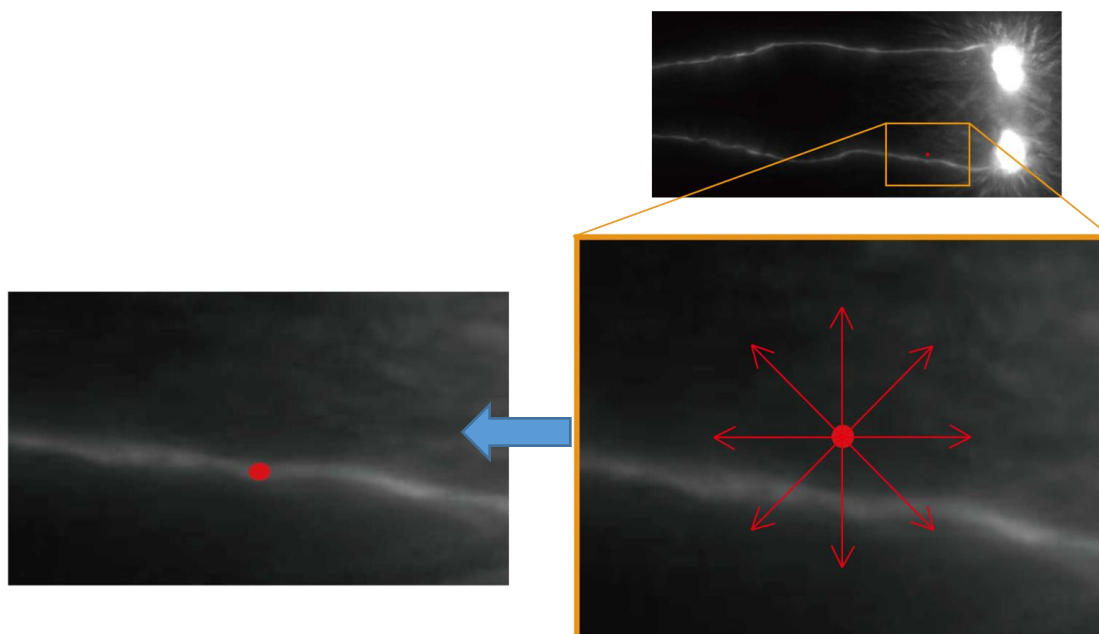


**Figure 28 The Scheme of Our Live Feedback Algorithm**

## 2. TakeDifferentIntensityImages

This is a straightforward macro; it automatically changes the illumination intensity to some defined values while taking images under those defined illumination intensities, and saves those images with distinguishable names, like CG118B-1-80%-Jan8-2019.jp2. We used this macro to take the 10%, 40% and 80% intensity of images listed in chapter 3.2.4.

Without this macro, in order to take different intensities of images, we need to manually change the illumination intensity to a specific value, take the image, and then save it. This time-consuming procedure photobleaches the sample remarkably, which will cause our emission intensity based responsivity segmentation algorithm to fail.

Along with those two major macros described above, we have coded tens of other useful macros. Most of those macros are simple but make the microscope controlling and image acquiring much easier.

In the future, we will transplant those macros to Matlab, because we will use Matlab to control every device in our lab, with those macros becoming just new functions in the

Matlab GUI or App.

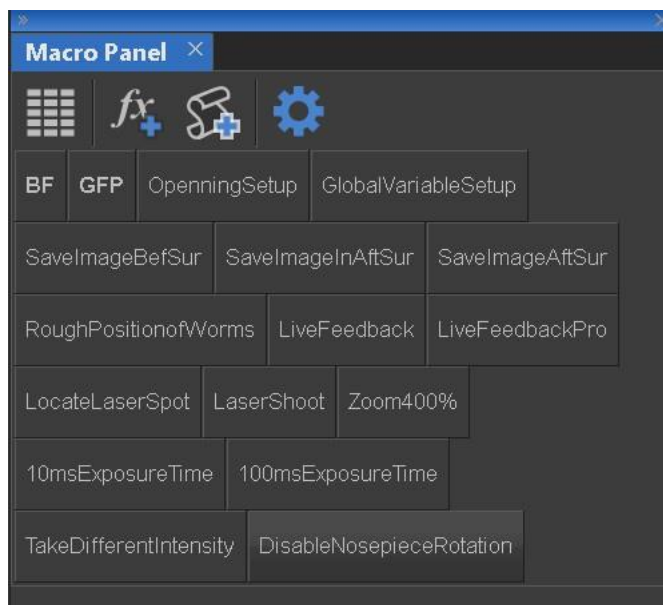


**Figure 29** The Macro Pane in Our Nikon NIS-Elements

## 6.2 Nikon Software Development Kit (SDK)

We already have the powerful Nikon NIS-Elements for Nikon Ti2 microscope and macros coded. Still, when encountering more complicated jobs, such as worm identification, imaging processing and controlling third-party devices, the NIS-Elements shows its weakness. Thus, we plan to do everything in Matlab, considering its versatile function, abundant resource, multiple toolboxes available, and the flexibility to transplant our result to other labs.

We will use Matlab to at least control our Nikon Ti2 inverted microscope, Leica M205 FA upright stereomicroscope, Andor cameras and femtoseconds laser. Our first step is trying to control the Nikon Ti2 using Matlab, utilizing the SDK provided by Nikon Instrument.

The SDK provides many functions written in C++ language. Those functions can control every part of the microscope independently. We found the interface program

between those C++ files and Matlab, and wrote a Nikon microscope controlling App in Matlab App designer. This App is currently in a testing phase to see whether we can control the microscope in Matlab (**Figure 30**).

We were able to use this App to control the stage movement, adjust beam path, switch objective, control turret and its shutter, change illumination intensity, and acquire images, of the microscope.

This App would allow direct data transfer from the microscope to Matlab, without exporting and importing using a separate software. This will make live image processing possible and our future jobs smoother.

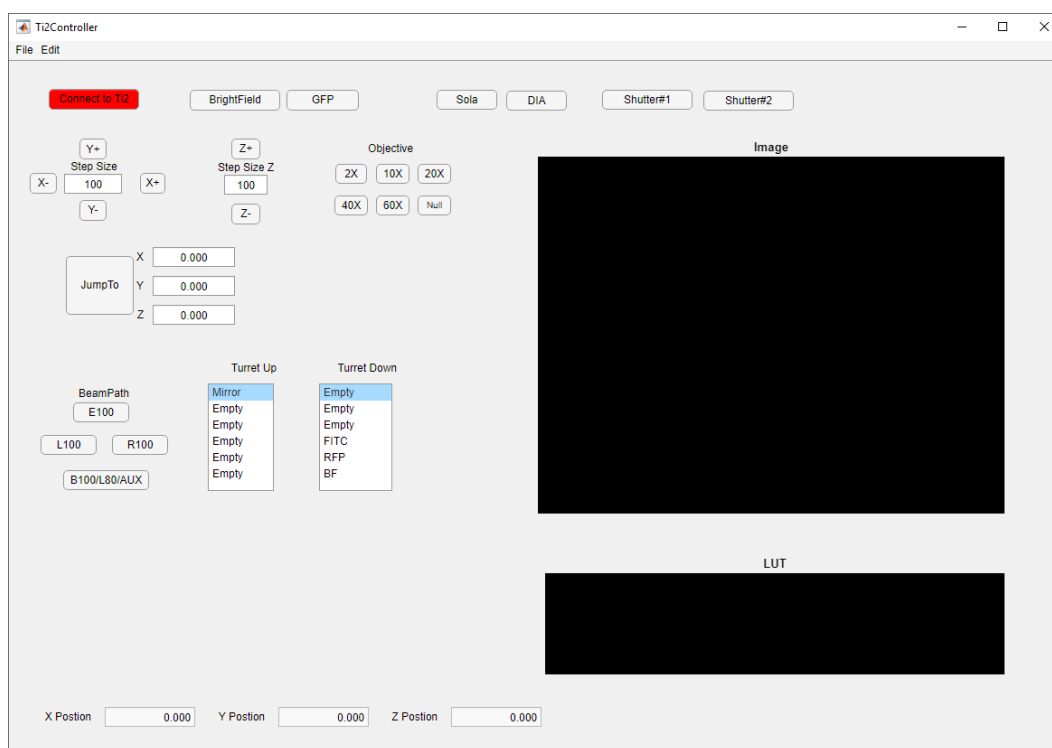


**Figure 30 Microscope Controlling App Designed in Matlab App Designer**